

Single Shot Solar Spectroscopic Design Aspects

A thesis submitted to the



**Department of Applied Optics & Photonics
University of Calcutta**

In the partial fulfillment of the requirements
for the award of the degree of
Master of Technology
In
Astronomical Instrumentation

By

Harsh Mathur

Under the guidance of

Dr. K. Nagaraju
Dr. K. Sankarasubramanian
Dr. Shibu K. Mathew



Indian Institute of Astrophysics, Bangalore

Declaration

I hereby declare that the thesis entitled “Single Shot Solar Spectroscopic Design Aspects” submitted to the University of Calcutta in the Department of Applied Optics and Photonics, in partial fulfillment of the requirements for the award of the degree of Master of Technology, is a result of the project work carried out by me at Indian Institute of Astrophysics, Bangalore, under the supervision of Dr K. Nagaraju (IIA), Dr K. Sankarabramanian (ISRO) and Dr. Shibu K. Mathew (USO). The results presented herein have not been subject to scrutiny, by any university or institute, for the award of a degree, diploma, associateship or fellowship whatsoever.

Harsh Mathur

Date:
Indian Institute of Astrophysics Bangalore-560034
India

Certificate

This is to certify that the thesis entitled “Single Shot Solar Spectroscopic Design Aspects” submitted to the University of Calcutta by Mr. Harsh Mathur in partial fulfillment of the requirements for the award of the degree of Master of Technology in Astronomical Instrumentation is based on the results of the project work carried out by him under my supervision and guidance, at the Indian Institute of Astrophysics. This thesis has not been submitted for the award of any degree, diploma, associateship, fellowship, etc. of any university or institute.

Dr K. Nagaraju

Dr K. Sankarsubramanian

Date:
Indian Institute of Astrophysics Bangalore-560034
India

“There's no such thing as perfect writing,
just like there's no such thing as perfect despair.”

--Haruki Murakami

Acknowledgments

I'd like to express my sincere gratitude to Dr. K. Nagaraju, Dr. K. Sankarsubramanian, Dr. Shibu K. Mathew for taking me up with this project. I'd like to acknowledge and thank Nagaraju for keeping up with my impatient nature and helping me work on being more patient. I also like to acknowledge and express my gratitude for taking the time to clear my doubts regarding the project and concepts in radiative transfer and spectropolarimetry. I'd like to thank Sankarsubramanian Sir for the detailed discussions about the DKIST snapshot spectrograph design and other discussions on relevant topics. I'd like to thank Shibu for inviting me to Udaipur and helping me with instrumentation, camera programs, serial port interfacing, etc. I'd also like to thank Dr. Raja Bayanna for helping me optimize Zeemax designs and designing achromats and helping me with setting up the instrument. I'd like to thank Dr. Dipankar Banerjee for the discussions about solar physics topics including but not limited to the solar atmosphere, waves, etc. I'd like to thank Sriram Sir for his invaluable insight in modeling and analyzing the performance of microlens arrays. I'd also like to acknowledge and thank Totan Sir for his constant help and involvement in designing the achromats.

Next, I'd like to thank my seniors Dr. Hemanth Pruthvi for helping me with spectro-polarimetry concepts and software interfacing with instruments. I'd like to thank my senior Dr. Mohan for the explanations about the snapshot spectrograph data reduction process and clearing other doubts as I had. I'd also like to thank my senior Souvik Bose for the discussions and explanations about sunspots and radiative transfer and for motivating me. I'd like to thank my senior Phanindra for helping me in the Optics lab with the instrument. I'd like to thank my senior Dr. Subhamoy for his ideas in optimizing the Zeemax design and image processing. I'd like to thank my senior Ritesh Patel for helping me time to time with reports and presentations. I'd like to thank Bibhuti and Kamlesh for the helpful discussions and explanations. I'd like to thank my batchmates Sarthak, Kshitij, Soumya, Pruthvi, Bharat and Vishnu for their constant involvement and support. I'd also like to thank my friends Ankit and Siddharth for moral support and being the pillars of strength while I made this career move.

I'm grateful towards Dr. Ravindra Banyal, Dr. Mousami Das and Dr. Subinoy Das for their invaluable classes. I'm grateful towards our BGS coordinator Dr. Ravindra and BGS Chair Dr. Aruna Goswami and BGS assistant Sankar Sir for their support.

I'd like to thank the computer support team to help me with troubleshooting systems and software whenever needed.

I'd also like to thank faculties from Calcutta University namely Prof. K. Bhattachaya, Prof. A. Ghosh, Prof. L.N. Hazra, Prof. A.B.Ray, Prof. S. Sarkar, Prof. A. Chakrabarty, Dr. R. Chakraborty, Dr. M. Ray for their wonderful teaching. I'd like to thank Dr. N. Chakraborty for their classes.

Above all, I'd like to thank my parents for their constant support, love, and blessings. I'd like to thank my brother Vibhor for being a pillar of strength and taking the responsibility of my parents for me to freely pursue the studies.

Abstract

High time-cadence Spectro-Polarimetry allows the feasibility of studying magnetic field evolution coupled with the plasma flows. Such a high cadence solar spectro-polarimetry if developed will allow one to study magnetic field evolution in eruptive processes like solar flares, prominence eruptions, etc. A single shot solar spectroscopy was recently demonstrated at Multi-application Solar Telescope (MAST) at Udaipur Solar Observatory. The snapshot spectroscopy is performed by sampling the pupil plane using the lenslet array to get multiple images of the field of view (FOV), which are then collimated and the collimated beam is made to pass through an FP Etalon in collimated mode. As the distance from the FP axis increases, the peak transmitted wavelength shift towards the bluer side. Using a pre-filter with a full width half maximum (FWHM) less than the free spectral range (FSR) of FP, combined with an imaging lens, we can get multiple images of FOV on image plane with a blue shift in spectra as we move radially outwards from the optical axis.

We have made an optimized Zeemax design utilizing the above concept for Multi-application Solar Telescope (MAST) at Udaipur Solar Observatory and also demonstrated the concept using available components and collected sample data.

We have made a Zeemax design of the Snapshot Spectrograph for the Daniel K. Inouye Solar Telescope (DKIST), carried out tolerance analysis through Monte-Carlo simulations and presented the Spot diagrams and PSF for the worst and best case scenarios.

We have also attempted to demonstrate snapshot spectro-polarimetric concepts in IIA Optics Lab. We have used Stokes definition polarimeter i.e. a linear analyzer and a quarter wave plate combination as a polarimeter. We have used He-Ne laser followed by a linear polarizer as a light source and collimated it from a 50-micron pinhole, the collimated beam is incident upon the lenslet array making multiple images of the pinhole, images are further collimated and made to pass through the FP and imaged at the detector. We have presented the results of this experiment i.e. Stokes parameters.

Contents

Declaration	2
Certificate	3
Acknowledgments	4
Abstract	6
Contents	7
List of Figures	9
List of Tables	11
1 Introduction	12
1.1 Traditional Methods of Spectroscopy	12
1.1.1 Push broom scanning	12
1.1.2 1D line scanning	13
1.1.3 Wavelength scanning	13
1.2 Hyperspectral Image	13
1.3 Snapshot Hyperspectral Techniques in Astronomy	14
1.3.1 Snapshot Spectroscopy with faceted mirrors	14
1.3.2 Snapshot Spectroscopy with lenslets on the image plane	15
1.3.3 Snapshot Spectroscopy with a fiber bundle	16
1.5 Structure of this Thesis	16
2 Snapshot Spectrograph Designs	18
2.1 Optical design for pupil sampling Snapshot Spectrograph	18
2.2 50 cm Telescope at MAST	19
2.3 Snapshot Spectrograph for Multi Application Solar Telescope (MAST)	20
2.3.1 Point Spread Function	21
2.3.2 RMS Wavefront Error	22
2.3.3 Spot Diagram	24
2.3.4 Design Parameters for Snapshot Spectrograph for MAST	24
2.3.5 Angle Distribution at image plane due to FP for MAST	25
2.4 Daniel K. Inouye Solar Telescope (DKIST)	26
2.5 Snapshot Spectrograph design for DKIST	29

2.5.1 Specifications	29
2.5.2 Achromatic Doublet Designs	30
2.5.2.1 First Imaging Lens (T)	30
2.5.2.2 Collimating Lens (L1)	30
2.5.2.3 Micro Lens Array	31
2.5.2.4 Collimating Lens (L2)	31
2.5.2.5 Imaging Lens (L3)	32
2.5.3 Pupil Sampling Snapshot Spectrograph Design for DKIST	33
2.5.4 Tolerance Analysis	33
2.5.4.1 Worst Case Point Spread Function (PSF)	35
2.5.4.2 Worst Case Spot Diagram	36
2.5.4.3 Worst Case RMS Wavefront Error	37
2.5.4.4 Best Case Point Spread Function (PSF)	38
2.5.4.5 Best Case Spot Diagram	39
2.5.4.6 Best Case RMS Wavefront Error	40
2.5.5 Design Parameters for Snapshot Spectrograph for DKIST	41
2.5.6 Angle Distribution at image plane due to FP for DKIST	41
2.6 Summary and Future Work	42
3 Instrumentation	43
3.1 Snapshot Spectrograph at MAST	43
3.2 Fabry Perot Etalon and Prefilter Calibration at MAST	44
3.3 Instrument Setup	46
3.4 Data Reduction	47
3.4.1 Flat Fielding	48
3.4.2 Line Profile from Data	50
3.5 Simulated Data	50
3.5.1 Simulated Profile	51
3.6 Snapshot Spectro-Polarimeter	52
3.6.1 Lab Snapshot Spectro-Polarimeter Setup	52
3.6.2 Data from Snapshot Polarimeter	53
3.7 Summary and Future Work	58
4 Summary and Future Work	59
5 References	60
Appendix A	62

List of Figures

Fig 1.1 Hyperspectral Data Cube	13
Fig 1.2 Facet mirror slicers divide the image and divert...	14
Fig 1.3 Lenslet array samples the image plane and the...	15
Fig 1.4 A fiber bundle samples a 2D image plane...	16
Fig. 2.1 Blue shift in transmitted wavelength	18
Fig. 2.2 Optical design for pupil sampling snapshot spectrograph	19
Fig 2.3 Optical layout and mechanical design of MAST	20
Fig 2.4 Pupil Sampling Snapshot Spectrograph Design for MAST	21
Fig 2.5 PSF of the Snapshot Spectrograph for MAST	22
Fig 2.6 RMS Wavefront error for different wavelength and fields for MAST	23
Fig 2.7 Spot Diagram for different wavelength and fields for MAST	24
Fig 2.8 Angles in degrees on the Detector for MAST	26
Fig 2.9 Gregorian Optics of DKIST	27
Fig 2.10 The Coudé Transfer Optics of DKIST	28
Fig 2.11 The Coudé Rotator Optics	28
Fig 2.12 Optical design of the Snapshot Spectrograph for DKIST	33
Fig 2.13 Worst case PSF during Monte Carlo Simulations for DKIST	35
Fig 2.14 Worst case Spot Diagram during Monte Carlo Simulations for DKIST	36
Fig 2.15 Worst case RMS Wavefront Error during Monte Carlo Simulations for DKIST	37
Fig 2.16 Best case PSF for DKIST	38
Fig 2.17 Best case Spot Diagram for DKIST	39
Fig 2.18 Best case RMS Wavefront Error for DKIST	40
Fig 2.19 Angles in degrees on the Detector for DKIST	42
Fig 3.1 A sample FP profile at step -100	44
Fig 3.2 FP Shift in Spectra with respect to the spectrum at step zero	45
Fig 3.3 Photo Showing the experimental setup of Snapshot Spectrograph at MAST	45
Fig 3.4 Spatio-spectral image plane and mask using Hough transform	47
Fig 3.5 Rows and Columns stacked to trace the path of absorption lines	48

Fig 3.6 Master Flat, Raw Data, and Corrected Data at step -150	49
Fig 3.7 Line profile at a point using observed data at step -150	50
Fig 3.8 Simulated Data at step -150	51
Fig 3.9 Line profile at a point using simulated data at step -150	51
Fig 3.10 Snapshot Spectro-polarimeter Lab Setup	53
Fig 3.11 Lenslet images without FP	54
Fig 3.12 Data at Linear polarizer 0-degree orientation	54
Fig 3.13 Stokes Images over different lenslets	55

List of Tables

Table 2.1 Optical Design Specification of Elements in Snapshot Spectrograph for MAST	20
Table 2.2 Parameters and values for MAST Snapshot Spectrograph	24
Table 2.3 Optical Prescription for different mirror surfaces of DKIST	27
Table 2.4 Optical Design Specifications of the elements of snapshot spectrograph for DKIST	29
Table 2.5 Optical Prescription of the first imaging lens (T) for DKIST	30
Table 2.6 Optical Prescription of the collimating (L1) lens for DKIST	30
Table 2.7 Optical Design Specification of the microlens array for DKIST	31
Table 2.8 Optical Prescription of the collimating (L2) lens for DKIST	31
Table 2.9 Optical Prescription of the imaging (L3) lens for DKIST	32
Table 2.10 Tolerance data for lenses for DKIST	33
Table 2.11 Abbe Tolerances of the material at different surfaces.	34
Table 2.12 Parameters and values for DKIST Spectrograph	41
Table 3.1 Optical Design specification of Snapshot Spectrograph installed at MAST	43
Table 3.2 FP Calibration Data	44
Table 3.3 Optical Design Specification of the Components used in IIA Optics Lab	52

1 Introduction

As we get better telescopes we get better resolution and time cadence, thus we are able to resolve and discover more magnetic features. Spectroscopy and spectropolarimetry are widely used techniques to understand the dynamics of the magnetic field and the evolution of different magnetic features both spatially and temporally. One example is magnetic bright points (BP) which exist in 200 km scales and have very fast evolving times. Magnetic bright points are small scale structures thought to trace intense kG magnetic concentrations. The BP motions can be used to measure the dynamic properties of magnetic flux tubes and their interaction with granular plasma. Random motions inside BPs can create Alfvén wave turbulence, which dissipates the waves in a coronal loop.

Another interesting magnetic phenomenon is solar flares. Solar flares are a sudden release of energy in the solar atmosphere, which is seen as intense variations in brightness. The evidence suggests that solar flares are magnetic reconnection events when the stored or built up magnetic energy is thrown out, which is why most solar flares are seen in active regions. Solar flares often but not always are followed by CME eruptions. Solar flares are classified as A, B, C, M, X in increasing order of peak X-ray flux. Solar flares happen on timescales of minutes to hours.

To understand the magnetic phenomenon and associated dynamics, we need spectropolarimetric information at very fast time scales over the full field of view (FOV). The traditional methods of spectroscopy although widely used have some limitations. As described in the following paragraphs, the technique has low time cadence, it can either capture FOV (2D spatial information) and scans over the line profile or captures the line information in one exposure but scans over the full field. The proposed snapshot spectroscopy technique neither scans in wavelength nor scans on the FOV but captures line information and spatial information in a single exposure.

1.1 Traditional Methods of Spectroscopy

1.1.1 Push broom scanning

A single spatial point is taken from a 2D spatial region and its spectrum is obtained through dispersers like prism or grating. Then a different spatial point is taken from the field to repeat the process. The scanning mechanism involves movement in x and y-direction to generate a spectral map of the whole field point by point which when combined forms a hyperspectral cube of the field. (Figure 1.1)

1.1.2 1D line scanning

This is a slit and grating-based spectrograph and the mechanism involves a slit which samples a 1D region of the 2D field and generates a wavelength map along with all the points in that 1D field. This slit is moved or raster scanned over the 2D field to generate a hypercube image of the field. (Figure 1.1)

1.1.3 Wavelength scanning

This method involves obtaining spatial information of a 2D image at a particular wavelength using narrow band filters or Fabry Perot interferometer (FP). The hyperspectral cube is obtained by scanning across the line by taking several images by tuning the filter or FP. (Figure 1.1)

1.2 Hyperspectral Image

Spectroscopy provides a plethora of information about the FOV. A spectral image of the field consists of two spatial dimensions (say x-direction and y-direction) and one spectral dimension (wavelength- λ). A data cube which is made up of two spatial and one spectral dimension is called a hyperspectral cube or Hyperspectral Image (HSI) and the dimensions are represented as $[x, y, \lambda]$ as shown in Figure 1.1.

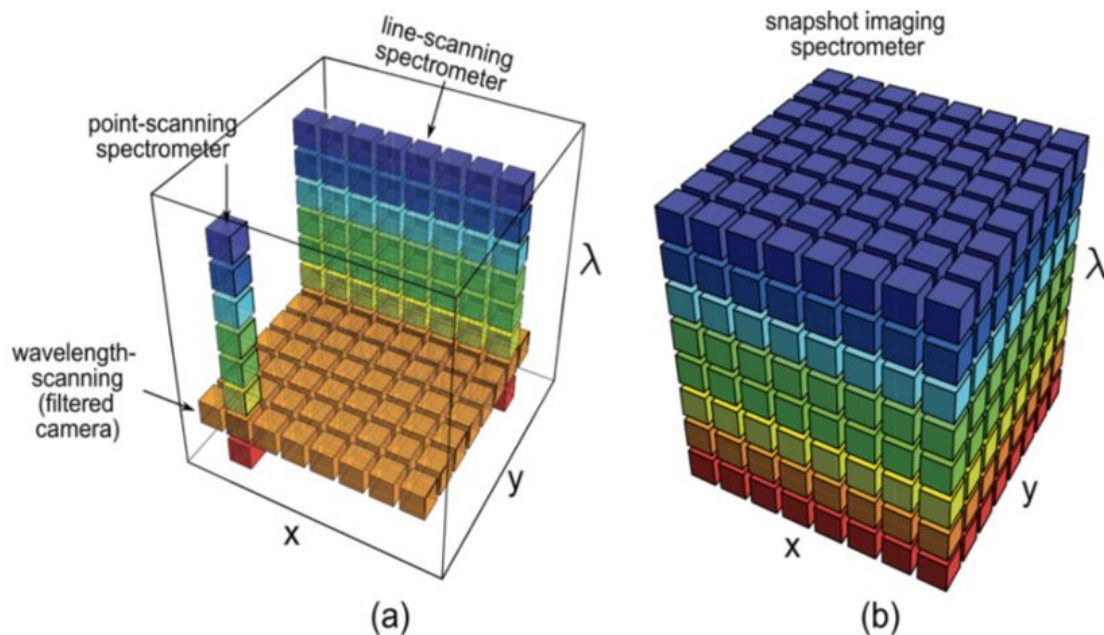


Fig 1.1. A hyperspectral data cube with the three-axis representing two spatial dimensions and one spectral dimension. (a) Represents the three scanning mechanisms commonly used to

generate a hyperspectral cube. (b) Represents a hypercube of an object consisting of the three dimensions $[x, y, \lambda]$ obtained in a snapshot

It is always necessary to generate the spectral information of an object before its spectral characteristics change or the object moves out of the field of view.

1.3 Snapshot Hyperspectral Techniques in Astronomy

Snapshot spectroscopy is a method of obtaining the hyperspectral cube in a single image frame i.e. a 3D data cube of $[x, y, \lambda]$ is generated using a 2D detector plane in a single exposure.

1.3.1 Snapshot Spectroscopy with faceted mirrors

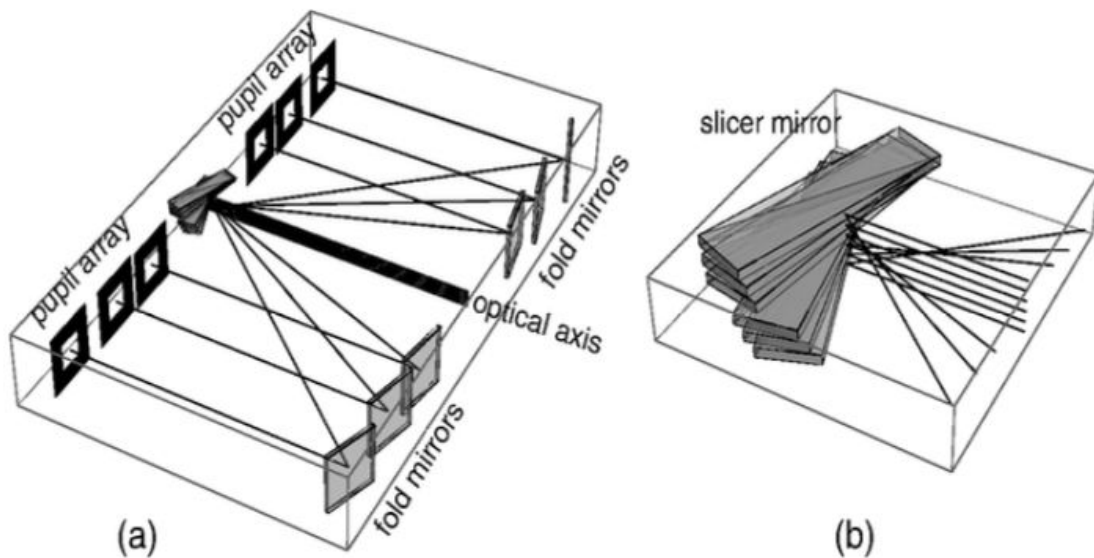


Fig 1.2 Facet mirror slicers divide the image and divert it into multiple spectrographs.

As shown in Figure 1.2, a set of closely spaced mirrors with slightly different angles such that an object whose image formed on this mirror is divided into several small regions. Each region is fed to separate spectrograph units and a spectrum is obtained. Then the divided regions and their respective spectra are combined to form Hyperspectral Image of the object.

1.3.2 Snapshot Spectroscopy with lenslets on the image plane

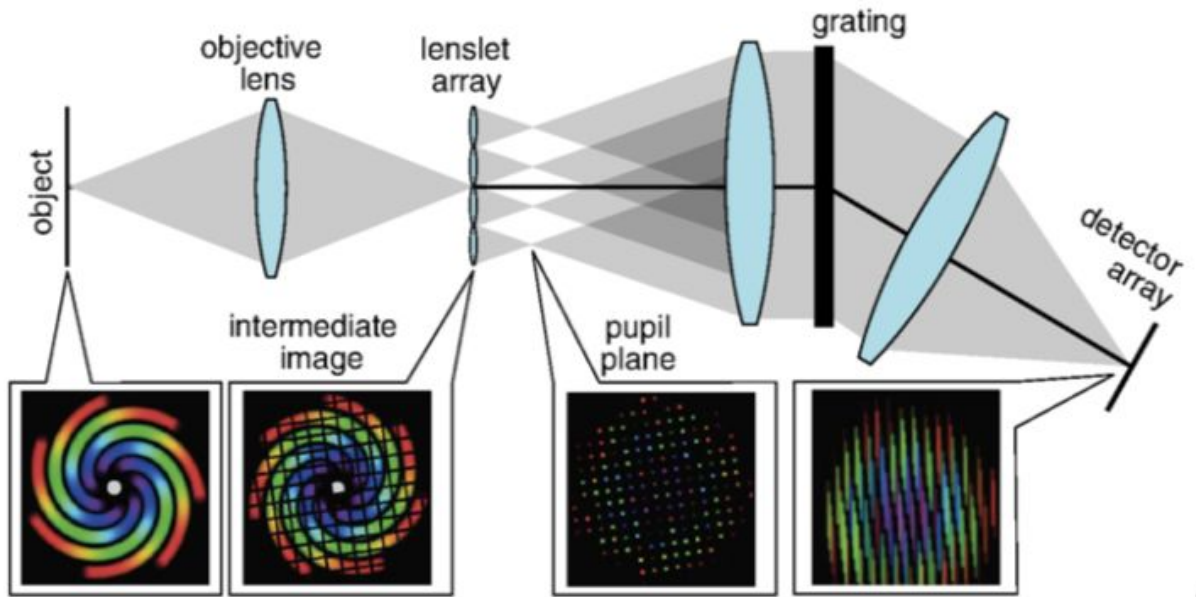


Fig 1.3 Lenslet array samples the image plane and the void created due to demagnification is used for spectral dispersion

An image of a 2D field formed by the telescope or an imaging lens is sampled by a set of lenslets (Figure 1.3). The image sampled by the lenslet gets shrunk or demagnified and occupies a small region with a void surrounding it. Each of the demagnified images is collimated and spectrally dispersed using a grating. The dispersed spectra when re-imaged forms a spectral streak of the demagnified image thus giving wavelength information at multiple points on the 2D field.

1.3.3 Snapshot Spectroscopy with a fiber bundle

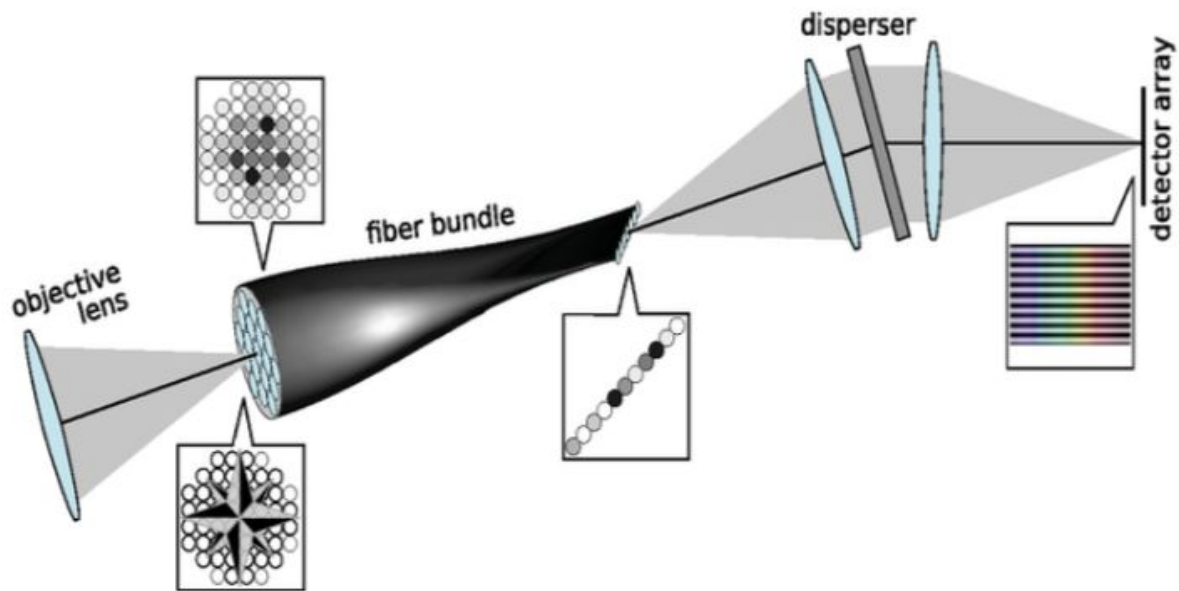


Fig 1.4 A fiber bundle samples a 2D image plane and re-formats it into 1D slit which is dispersed using a spectrograph

An optic fiber bundle is placed at the image plane of the telescope (Figure 1.4). The fibers are oriented in such a way that the 2D field sampled by the fibers are converted to 1D slit structure. A grating is used to obtain the spectra of the 1D slit. As we obtain the spectral information of every point on the 1D slit, we effectively have the spectra of the 2D image forming a hyperspectral image.

All the techniques mentioned above sample the image plane and uses a grating based spectrograph to obtain capabilities. A novel instrument technique is developed by sampling the pupil plane instead of the image plane and uses a Fabry-Perot interferometer as a spectral disperser.

1.5 Structure of this Thesis

Each chapter is independent of the contents from the other chapters and is self-sustained. As the chapters talk about instruments or designs, the conclusion of the chapters also contains possible improvements and future work of those instruments. The second chapter discusses the Zeemax design for MAST and DKIST. It also talks about tolerances considered while designing the achromats. The third chapter discusses the snapshot spectroscopy technique demonstrated at

MAST and the data reduction technique. It also discusses the snapshot spectro-polarimetry experiment done at IIA and presents its results.

2 Snapshot Spectrograph Designs

2.1 Optical design for pupil sampling Snapshot Spectrograph

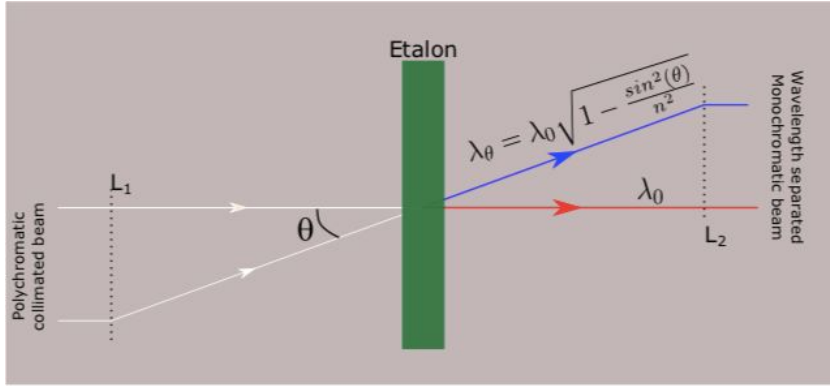


Fig. 2.1 Blue shift in transmitted wavelength for a ray traveling at an angle with respect to the ray traveling normal to the etalon

A schematic of the optical setup is displayed in Fig. 2.1. As shown in this figure the field of view (FOV) is limited using a field stop. The beam exiting the field stop is collimated using a lens L1 and the pupil image is formed behind L1 at a distance equal to its focal length. This pupil plane is sampled by a lenslet array to get individual identical images of the region of interest (ROI) at the focal plane of the lenslet (Shack Hartmann Image Plane). The lenslet images are re-collimated using lens L2, which is analogous to lens L1 in Fig. 2.2, and the beam is made to pass through an etalon at angles which are determined by the focal length of the lens L2 (f) and the distance of the object (d) from the optic axis according to the relation,

$$\theta = \tan^{-1} \left(\frac{d}{f} \right). \quad (2.1)$$

As the distance from the optic axis increases, the peak transmitted wavelength shift towards the bluer side. Since the system is symmetric along the radial direction, all points at the same radial distance from the optic axis are at the same wavelength. The wavelength decreases radially according to the relation,

$$\Delta\lambda = \left(\frac{\lambda_0}{2} \right) \times \left(\frac{\theta}{\mu} \right)^2. \quad (2.2)$$

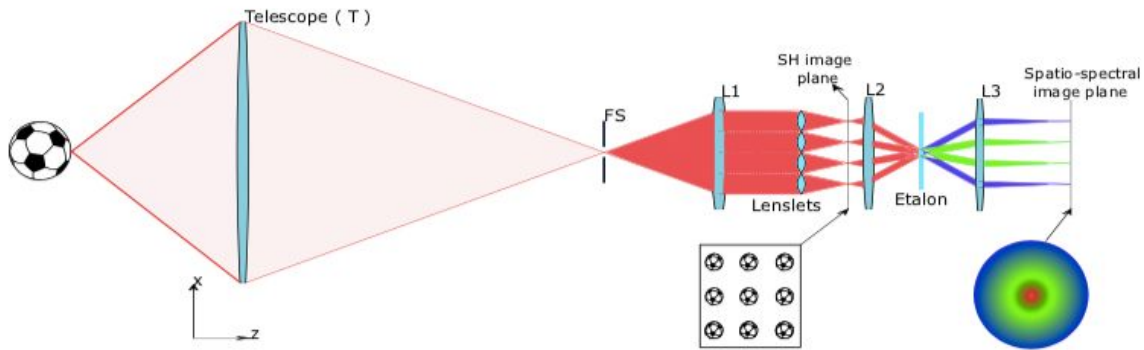


Fig. 2.2 Optical design for pupil sampling snapshot spectrograph

The wavelength sampled pupil is imaged using lens L3, which is analogous to lens L2 in Fig. 2.2, to get multiple images of the region of interest onto the spatio-spectral image plane. Hence, we get multiple images of ROI sampled at different wavelengths to get a hyperspectral image of the object at the spatio-spectral image plane.

2.2 50 cm Telescope at MAST

The MAST telescope is an off-axis Gregorian type with 50 cm aperture. The primary mirror (M1) is made of Zerodur and has a focal length of 2 m (focal number = 4). Fig. 2.3 shows the optical layout (a) and the mechanical design (b) of the telescope. The field stop placed at prime focus allows 6 arcmin field-of-view to pass through the remaining optics. The secondary mirror (M2) placed close to the field stop collimates the light. The Coude train, which consists of three mirrors (M3, M4, and M5), sends the beam vertically down to the observing room. The telescope is placed on an alt-azimuth mount and thus causes image rotation. The beam is sent through an image derotator (M6, M7, and M8) before reaching the folding mirror M9. From M9 the collimated beam is sent to the back-end instruments in the observing room.

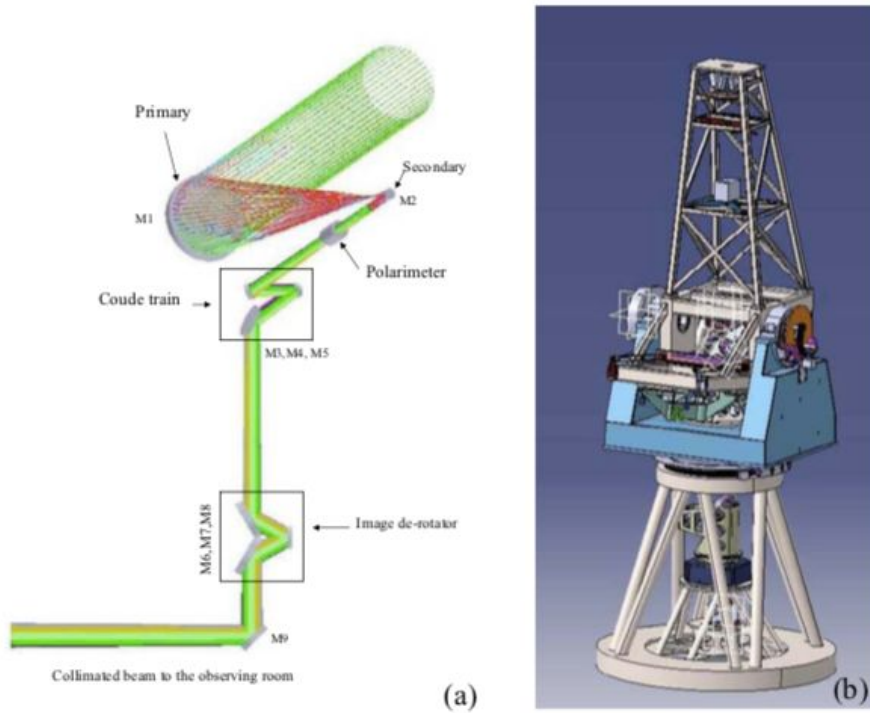


Fig 2.3 Optical layout (a) and the mechanical design (b) of the MAST telescope (courtesy: AMOS, Belgium).

2.3 Snapshot Spectrograph for Multi Application Solar Telescope (MAST)

The following off-the-shelf elements are used in the pupil sampling spectrograph design for MAST.

Table 2.1 Optical Design Specification of Elements in Snapshot Spectrograph for MAST

Element	Specification	Vendor and Model
Telescope (T) Aperture	90 mm	Edmund Optics #54-567
Telescope (T) Focal Length	849.9 mm	
Field Stop	3.858 mm	
L1 Focal Length	175 mm	Edmund Optics #49-363

SH Lenslet Pitch	1 mm	
SH Lenslet Focal Length	45 mm	
L2 Focal Length	200 mm	Edmund Optics #88-596
Fabry Perot Type	Air-Spaced Etalon	
FP FSR and FWHM	3.75 Å and 235 mÅ	
L3 Focal Length	150 mm	Edmund Optics #49-391
FOV	1.5 arcmin	

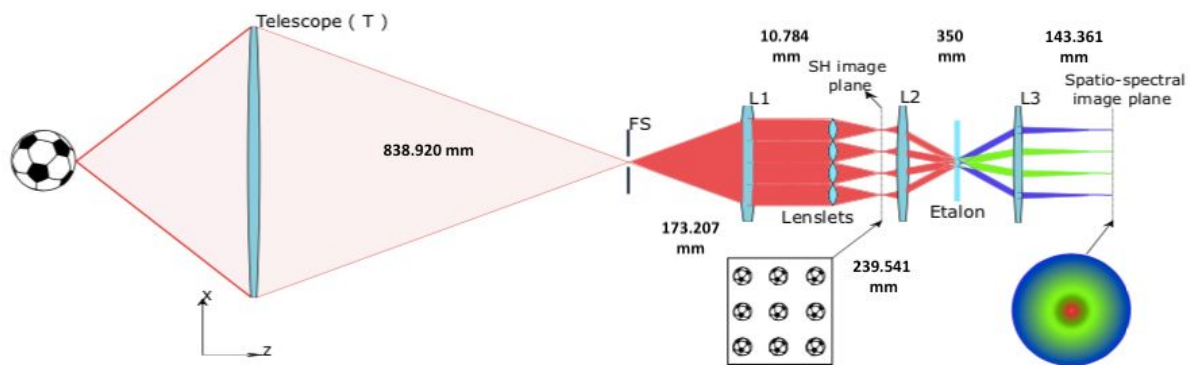


Fig 2.4 Pupil Sampling Snapshot Spectrograph Design for MAST

2.3.1 Point Spread Function

The point spread function (PSF) describes the response of an imaging system to a point source or point object. A more general term for the PSF is a system's impulse response, the PSF being the impulse response of a focused optical system.

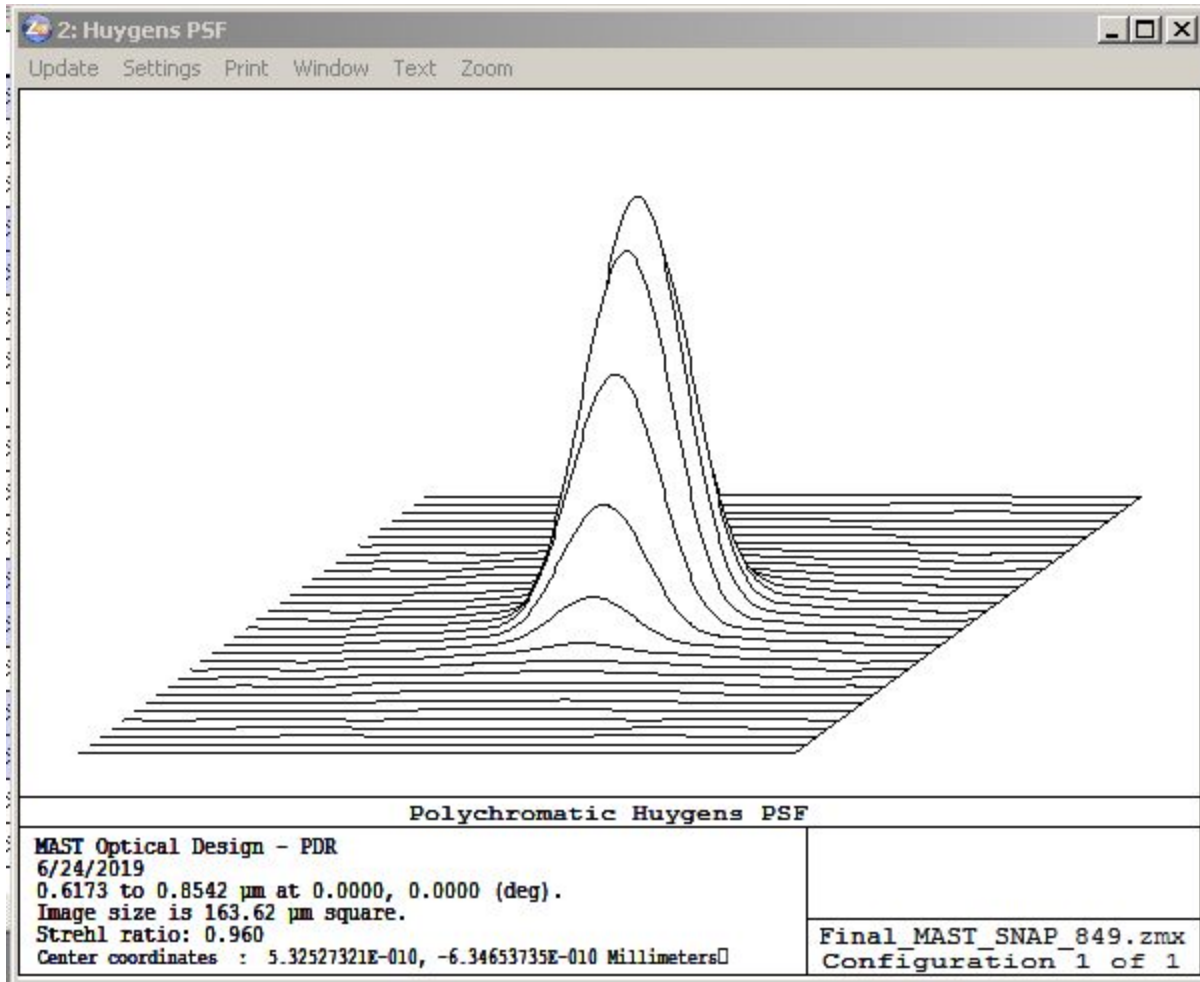


Fig 2.5 PSF of the Snapshot Spectrograph for MAST

Figure 2.5 displays the point spread function (PSF) for the pupil sampling spectrograph for MAST. The Strehl ratio is 0.960.

2.3.2 RMS Wavefront Error

The root-mean-square wavefront error or RMS wavefront error is a specific average over the wavefront phase errors in the exit pupil.

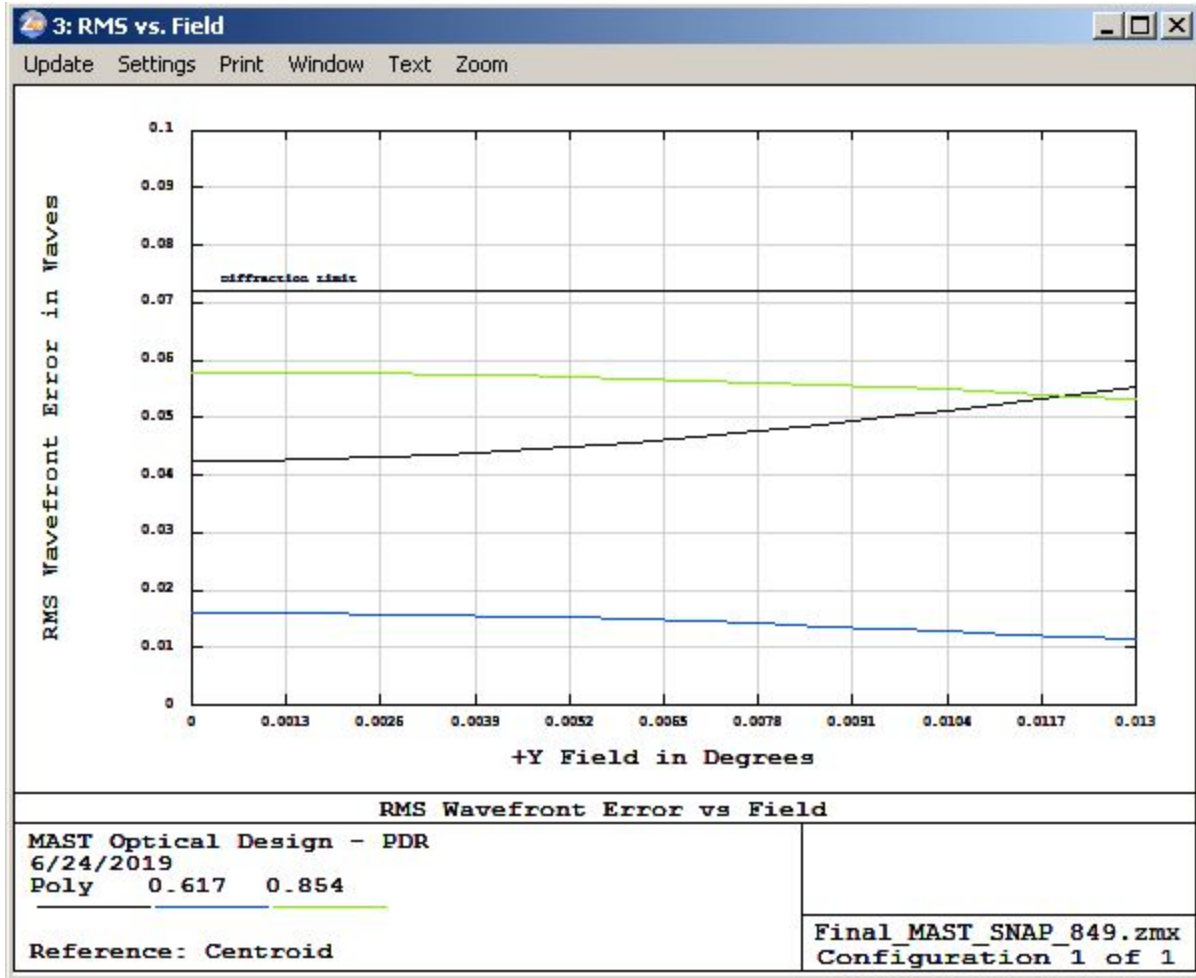


Fig 2.6 RMS Wavefront error for different wavelength and fields for MAST

Figure 2.6 displays the RMS wavefront error over the full field for MAST. We can see, it is below the diffraction limit.

2.3.3 Spot Diagram

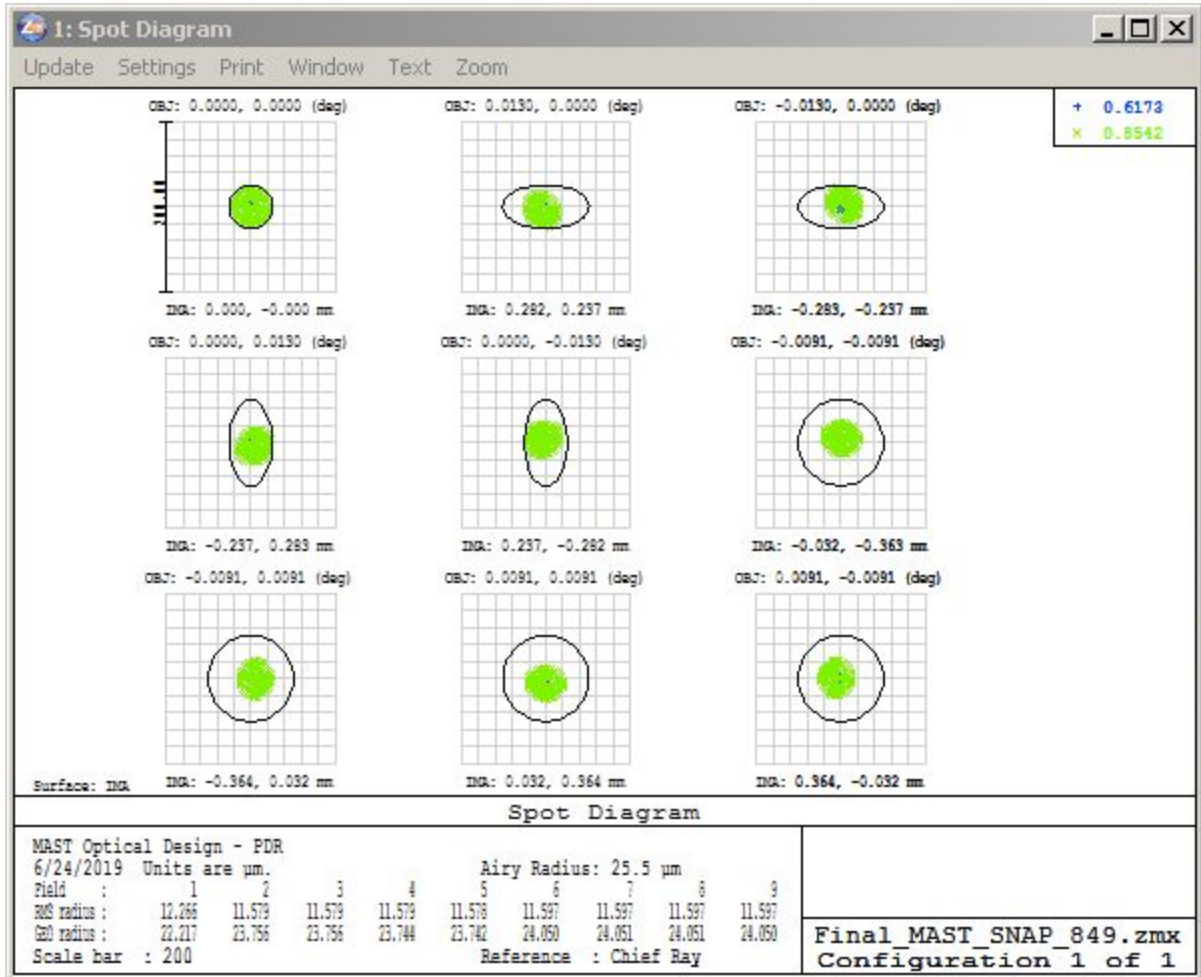


Fig 2.7 Spot Diagram for different wavelength and fields for MAST

Figure 2.7 displays the spot diagram over wavelengths 6302 Å and 8542 Å over different fields. We can see the maximum spot radius is 24.05 μm which is below the airy disc radius 25.5 μm .

2.3.4 Design Parameters for Snapshot Spectrograph for MAST

Table 2.2 Parameters and values for MAST Snapshot Spectrograph

Parameters	Values
------------	--------

Airy Disc Radius	25.5 μm
Spot Size	24.05 μm
Strehl Ratio	0.960
RMS Wavefront Error	0.06 waves

2.3.5 Angle Distribution at image plane due to FP for MAST

We have calculated angles at a 1k X 1k detector with 6.4 μm pixel size using the lenslet array as mentioned above.

We have assumed the detector axis is aligned with the principal axis of the system and the Fabry Perot. We have calculated angles at each pixel from the line joining the center of the imaging lens and the pixel with the principal axis. To calculate the microlens array mask, as given in Table 2.1, we have used a 1 mm pitch microlens array, 200 mm focal length collimating lens and 150 mm focal length imaging lens. We infer that because the system is centrally symmetric, at same radial distances from the detector center, the angles will be the same, and Hence according to equation 2.2, all pixels at the same radial distance will be at the same wavelength. We also note that the maximum angular variation is 1.4 degrees. Figure 2.8 shows the angle variation on the detector with the microlens array masks.

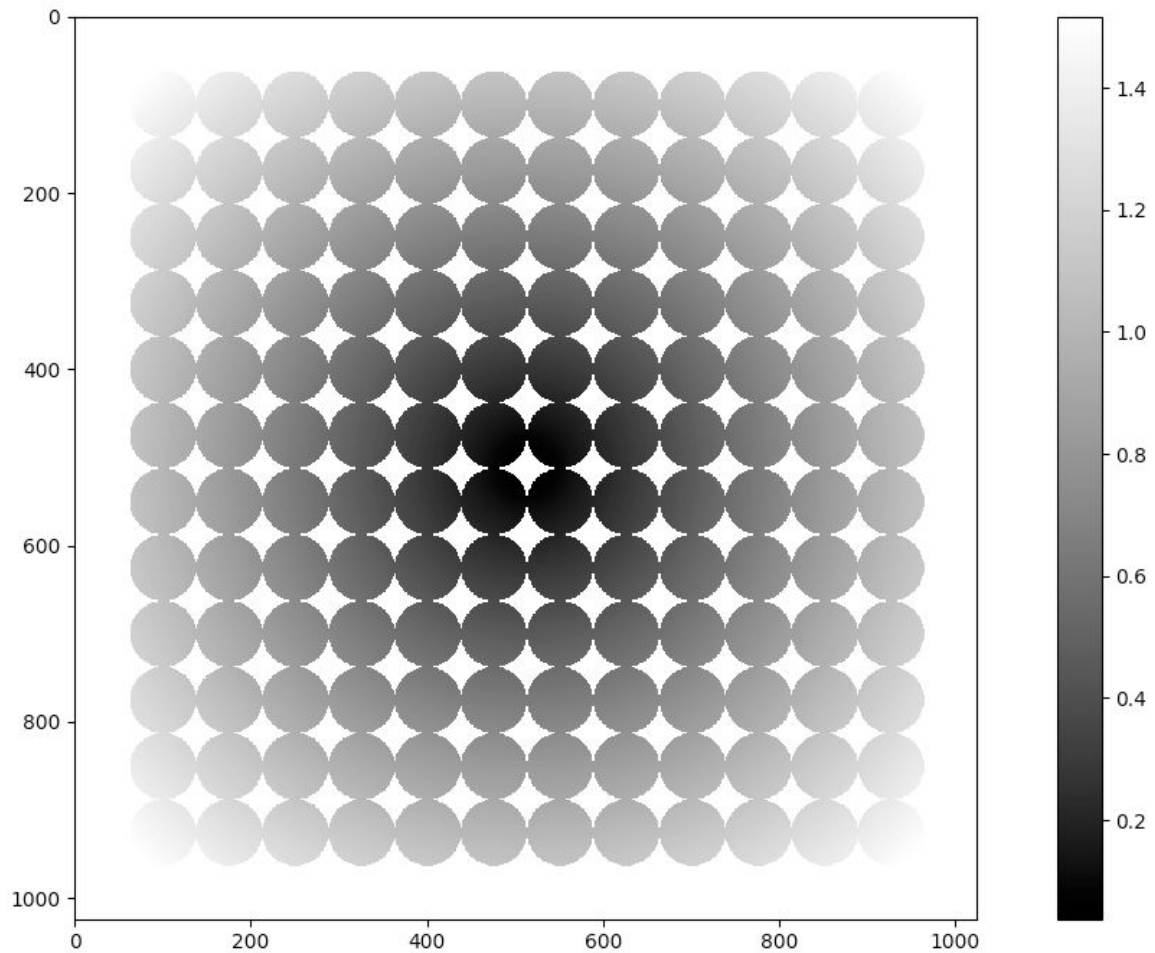


Fig 2.8 Angles in degrees on the Detector when 1k x 1k detector with 6.4 μm pixel size is used with microlens arrays with 1 mm pitch.

2.4 Daniel K. Inouye Solar Telescope (DKIST)

The DKIST is an off-axis Gregorian telescope (Hubbard, Robert [3]) with 4240 mm diameter primary mirror with aperture stop of 4000 mm with the radius of curvature 16000 mm. The secondary mirror has a radius of curvature of 2081.255 mm. These are followed by Coudé transfer optics which consists of a fold mirror and a relay mirror with a radius of curvature (ROC) 5979.243 mm. These are followed by mount base transfer optics (fold mirrors) and finally to Coudé Rotator optics which consists of fold mirror, a collimator (ROC 21442.354 mm) and a coma corrector and deformable mirror. (Figure 2.9, 2.10 and 2.11)

Table 2.3 Optical Prescription for different mirror surfaces of DKIST

Element		Conic Constant	Radius of Curvature (mm)	Curve
OSS Gregorian Optics				
M1	Primary	-1	16,000	Concave
M2	Secondary/FSM	-0.5393103	2,081.255	Concave
OSS Coudé Transfer Optics				
M3	Fold Mirror	-	-	Flat
M4	Relay Mirror	-0.3717299	5,979.243	Concave
Mount Base Assembly Coudé Transfer Optics				
M5	FSM	-	-	Flat
M6	Fold Mirror	-	-	Flat
Coudé Rotator Optics				
M7	Fold Mirror	-	-	Flat
M8	Collimator	-1	21,442.354	Concave
M9	Coma Corrector	-	-	Flat w/coma [†]
M10	Deformable Mirror	-	-	Flat
BS1	WFC Beam Splitter	-	-	Flat

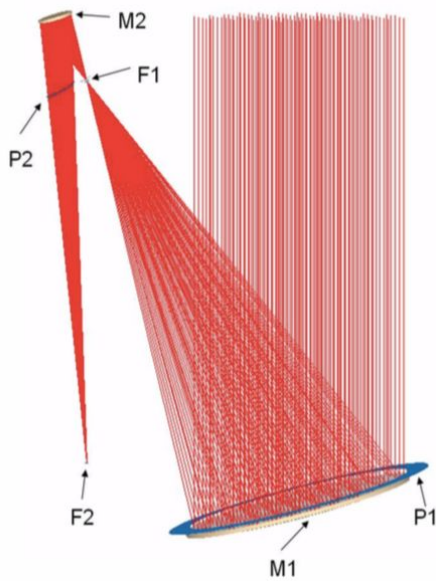


Fig 2.9 Gregorian Optics of DKIST (Hubbard, Robert [3])

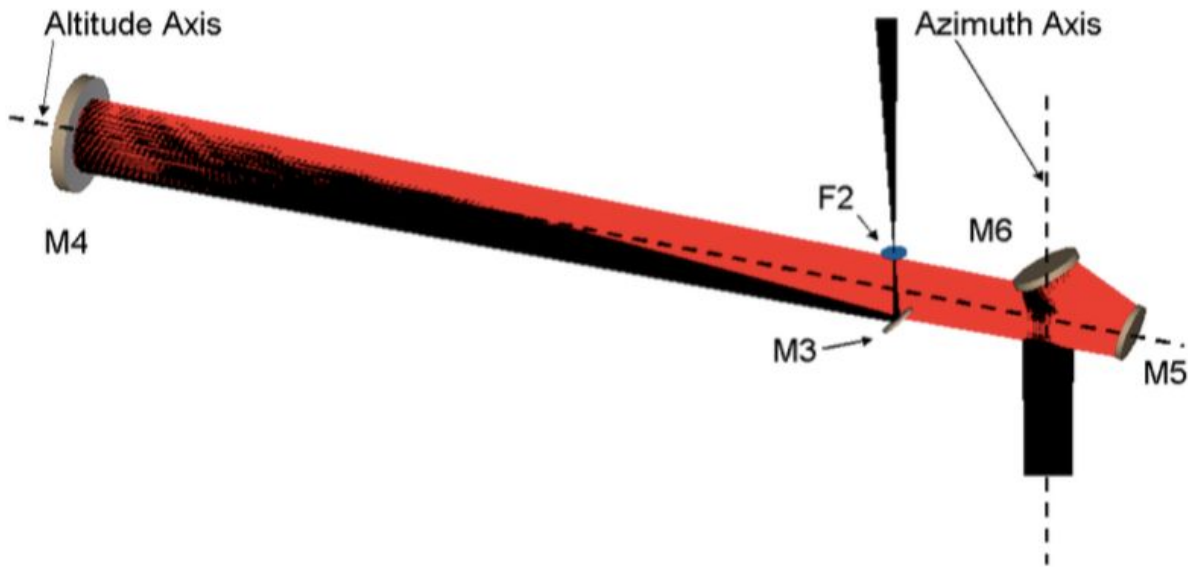


Fig 2.10 The Coudé Transfer Optics include two groups of components. The OSS group (M3 and M4) move with the Optical Support Structure as it rotates about the altitude axis. The other group consists of M5 and M6, which are fixed to the Mount Base Assembly. (Hubbard, Robert [3])

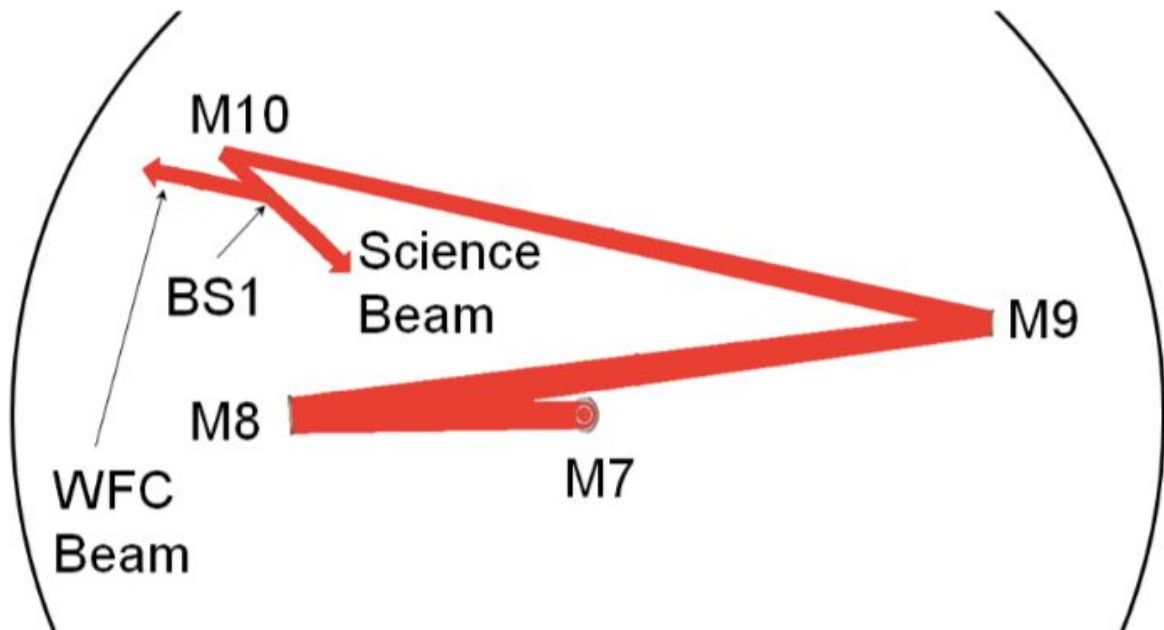


Fig 2.11 The Coudé Rotator Optics include M7 through M10 (the deformable mirror) and BS1, the beam splitter that reflects a small fraction of the beam into the wavefront correction system. (Hubbard, Robert [3])

2.5 Snapshot Spectrograph design for DKIST

We have designed four achromats, two for collimation(L1, L2) and two for imaging (T, L3) and selected an off-the-shelf microlens array. We have also optimized the distances between various components and have done the tolerance analysis to measure the tolerances over different parameters like the radius of curvature, tilts, distances between components and material purity (Abbe numbers). We are presenting an optical prescription for the achromats, the distance between components, worst and best case performance parameters like Spot Diagram, PSF and the RMS wavefront error.

2.5.1 Specifications

Table 2.4 Optical Design Specifications of the elements of snapshot spectrograph for DKIST

Element	Specification
Telescope (T) Aperture	280 mm
Telescope (T) Focal Length	3365 mm
Field Stop	14.026 mm
L1 Focal Length	175 mm
SH Lenslet Pitch	1.5 mm
SH Lenslet Focal Length	24.3 mm
L2 Focal Length	300 mm
Fabry Perot Type	Air-Spaced Etalon
FP FSR and FWHM	5 Å and 235 mÅ
L3 Focal Length	300 mm
FOV	30 arcsec

2.5.2 Achromatic Doublet Designs

2.5.2.1 First Imaging Lens (T)

Table 2.5 Optical Prescription of the first imaging lens (T) for DKIST

Element	Value
The radius of Curvature 1st Surface	1706.649 mm
The Radius of Curvature 2nd Surface	-838.721 mm
Thickness	40 mm
Material	N-PSK57
Air Gap	5 mm
The radius of Curvature 1st Surface	-840.782 mm
The radius of Curvature 2nd Surface	Infinity
Thickness	40 mm
Material	BAF9
Focal Length	3365 mm
Semi Diameter	140 mm

2.5.2.2 Collimating Lens (L1)

Table 2.6 Optical Prescription of the collimating (L1) lens for DKIST

Element	Value
The radius of Curvature 1st Surface	174.652 mm
The Radius of Curvature 2nd Surface	-69.191 mm

Thickness	10 mm
Material	P-PK53
Air Gap	0 mm
The radius of Curvature 1st Surface	-69.191 mm
The radius of Curvature 2nd Surface	-135.658 mm
Thickness	4 mm
Material	BAF9
Focal Length	175 mm
Semi Diameter	7.506 mm

2.5.2.3 Micro Lens Array

Table 2.7 Optical Design Specification of the microlens array for DKIST

Element	Value
Lenslet Model	Oko Tech APO-GB-P1500-F24.3 (633)
Pitch	1.5 mm
Focal Length	24.3 mm

2.5.2.4 Collimating Lens (L2)

Table 2.8 Optical Prescription of the collimating (L2) lens for DKIST

Element	Value
The radius of Curvature 1st Surface	331.023 mm

The radius of Curvature 2nd Surface	-81.369 mm
Thickness	13.59 mm
Material	BAK50
Air Gap	0 mm
The radius of Curvature 1st Surface	-81.369 mm
The Radius of Curvature 2nd Surface	-231.877 mm
Thickness	6 mm
Material	N-SF5
Focal Length	300 mm
Semi Diameter	21.831 mm

2.5.2.5 Imaging Lens (L3)

Table 2.9 Optical Prescription of the imaging (L3) lens for DKIST

Element	Value
The radius of Curvature 1st Surface	117.218 mm
The radius of Curvature 2nd Surface	-137.987 mm
Thickness	13.59 mm
Material	N-BK7
Air Gap	0 mm
The radius of Curvature 1st Surface	-137.987 mm
The radius of Curvature 2nd Surface	Infinity
Thickness	6 mm

Material	N-SF5
Focal Length	300 mm
Semi Diameter	20.006 mm

2.5.3 Pupil Sampling Snapshot Spectrograph Design for DKIST

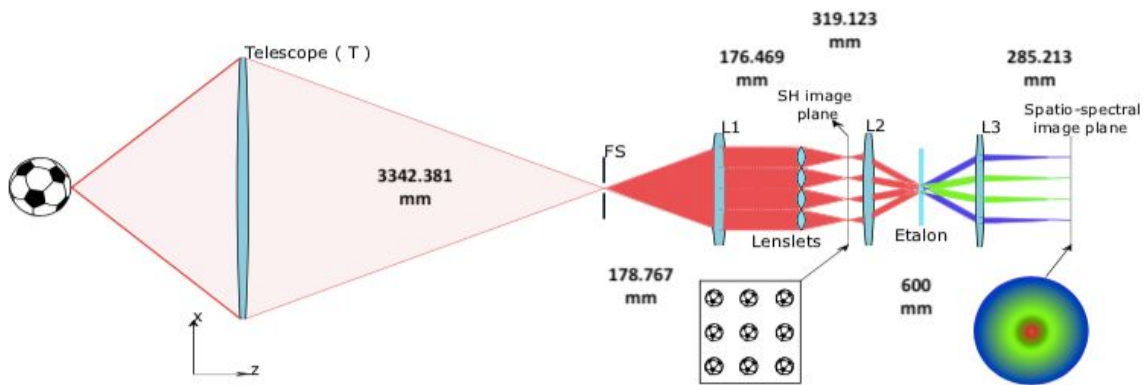


Fig 2.12 Optical design of the Snapshot Spectrograph for DKIST

Fig 2.12 displays the different components of the pupil sampling spectrograph with the distances between them.

2.5.4 Tolerance Analysis

The following tables (Table 2.10 and Table 2.11) present tolerances for various parameters in optical prescriptions of lenses and the design of snapshot spectrograph.

Table 2.10 Tolerance data for lenses for DKIST

Element	Tolerances
Radius of Curvature	+/- 0.125 mm
Thickness	+/- 0.05 mm

Tilt	+/- 0.05 degrees
------	------------------

Table 2.11 Abbe Tolerances of the material at different surfaces.

Abbe Number	Min	Max
68.399	-0.171	0.171
47.958	-0.120	0.120
66.220	-0.166	0.166
28.533	-0.071	0.071
57.990	-0.145	0.145
32.251	-0.081	0.081
64.167	-0.160	0.160
32.251	-0.081	0.081

Appendix A has detailed tolerance analysis results.

We have considered variation in point spread function (PSF), the Strehl ratio, spot radius, and RMS wavefront error to judge a Monte-Carlo simulation performance. Table 2.12 summarises the worst case and best case values of the above parameters.

2.5.4.1 Worst Case Point Spread Function (PSF)

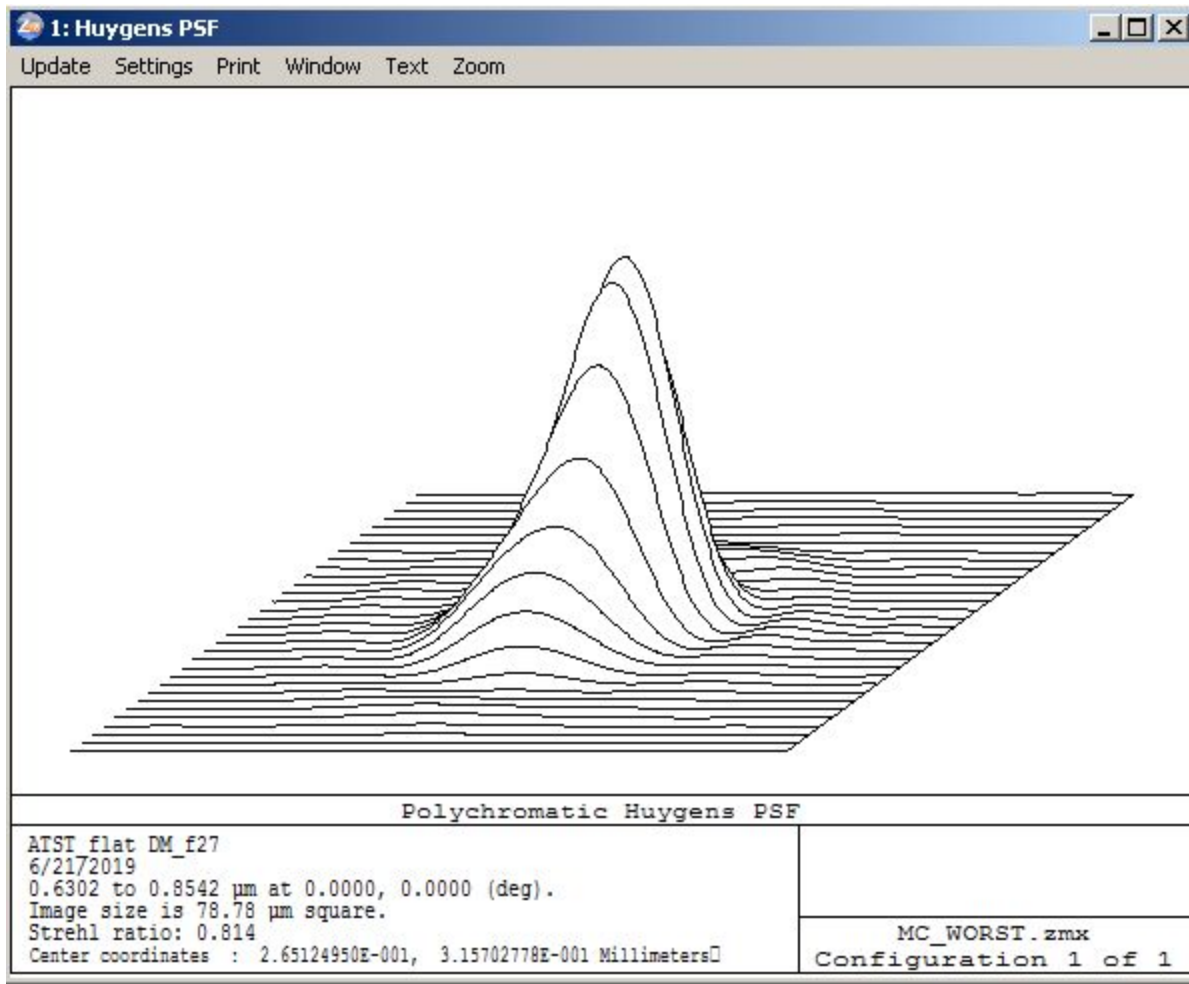


Fig 2.13 Worst case PSF during Monte Carlo Simulations for DKIST

Figure 2.13 displays PSF of the worst PSF attained during the Monte-Carlo simulations. The Strehl ratio is degraded to 0.814 from 0.981.

2.5.4.2 Worst Case Spot Diagram

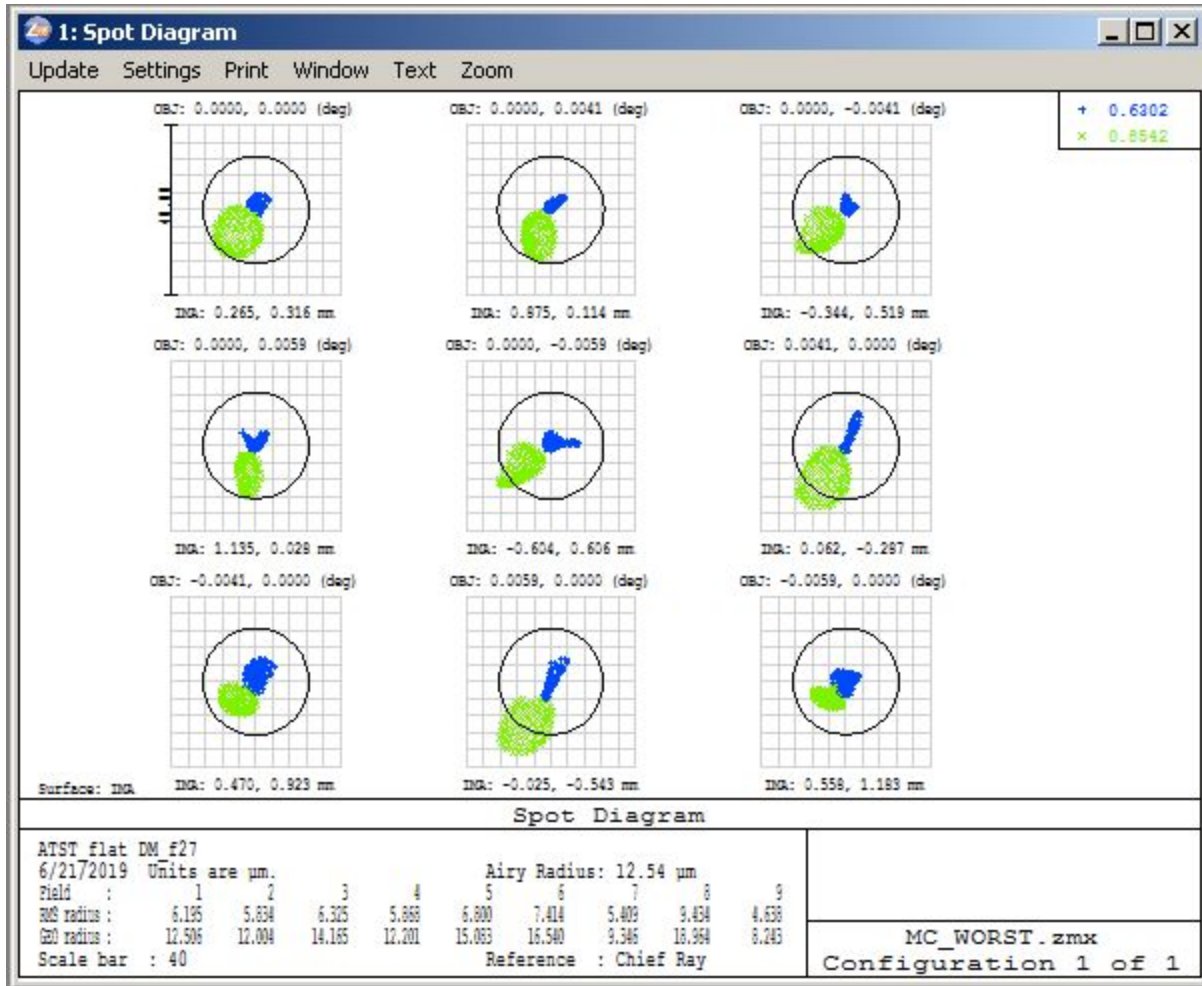


Fig 2.14 Worst case Spot Diagram during Monte Carlo Simulations for DKIST

Figure 2.14 displays Spot Diagram of the worst spot diagram attained during the Monte-Carlo simulations. The spot radius is degraded to 18 μm from 7 μm .

2.5.4.3 Worst Case RMS Wavefront Error

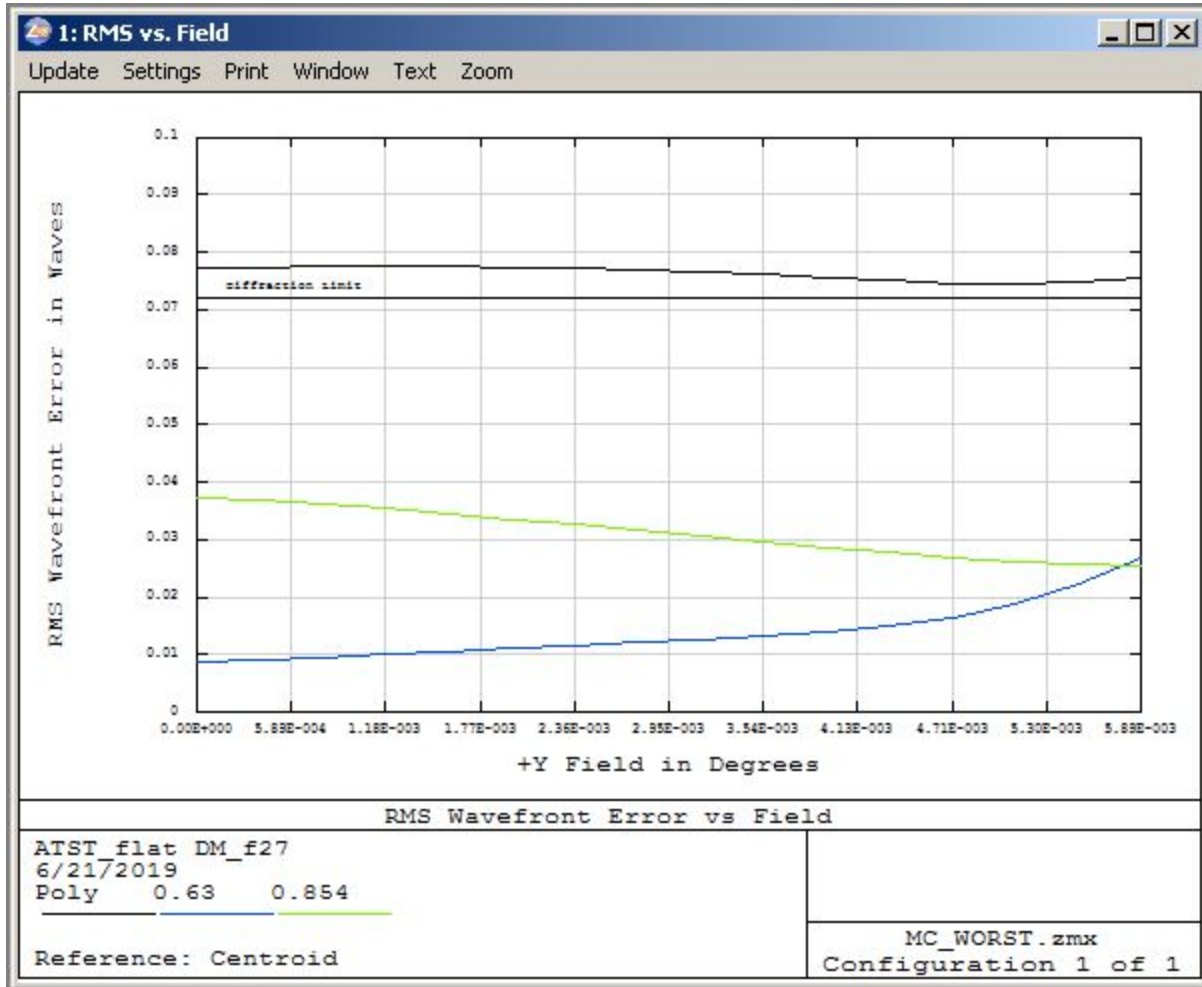


Fig 2.15 Worst case RMS Wavefront Error during Monte Carlo Simulations for DKIST

Figure 2.15 displays RMS wavefront error of the worst RMS wavefront error attained during the Monte-Carlo simulations. The RMS wavefront error is degraded to 0.08 waves from 0.04 waves.

2.5.4.4 Best Case Point Spread Function (PSF)

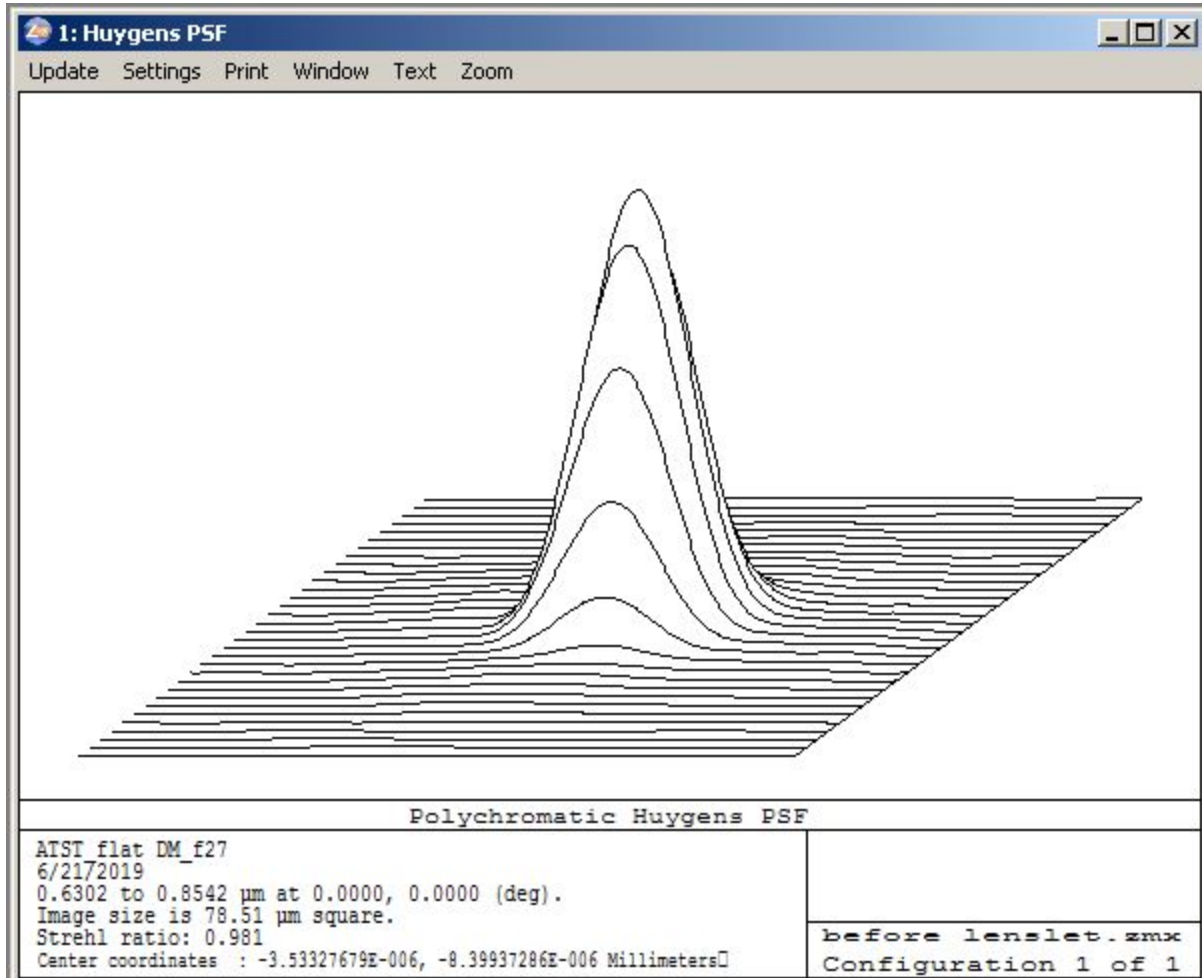


Fig 2.16 Best case PSF for DKIST

Figure 2.16 displaying best PSF attained with the Strehl ratio 0.981.

2.5.4.5 Best Case Spot Diagram

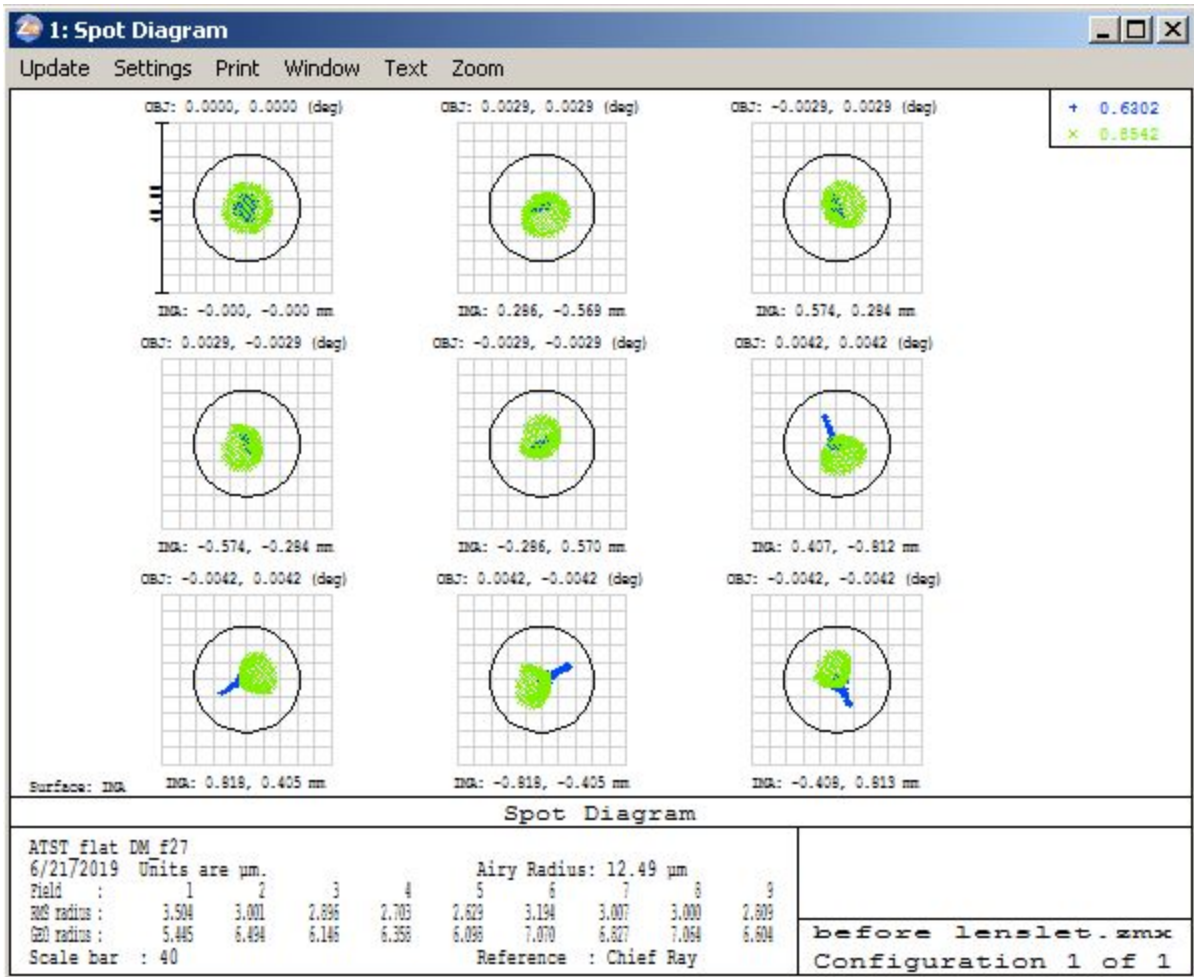


Fig 2.17 Best case Spot Diagram for DKIST

Figure 2.17 displaying best Spot radius attained with the spot radius 7.07 μm .

2.5.4.6 Best Case RMS Wavefront Error

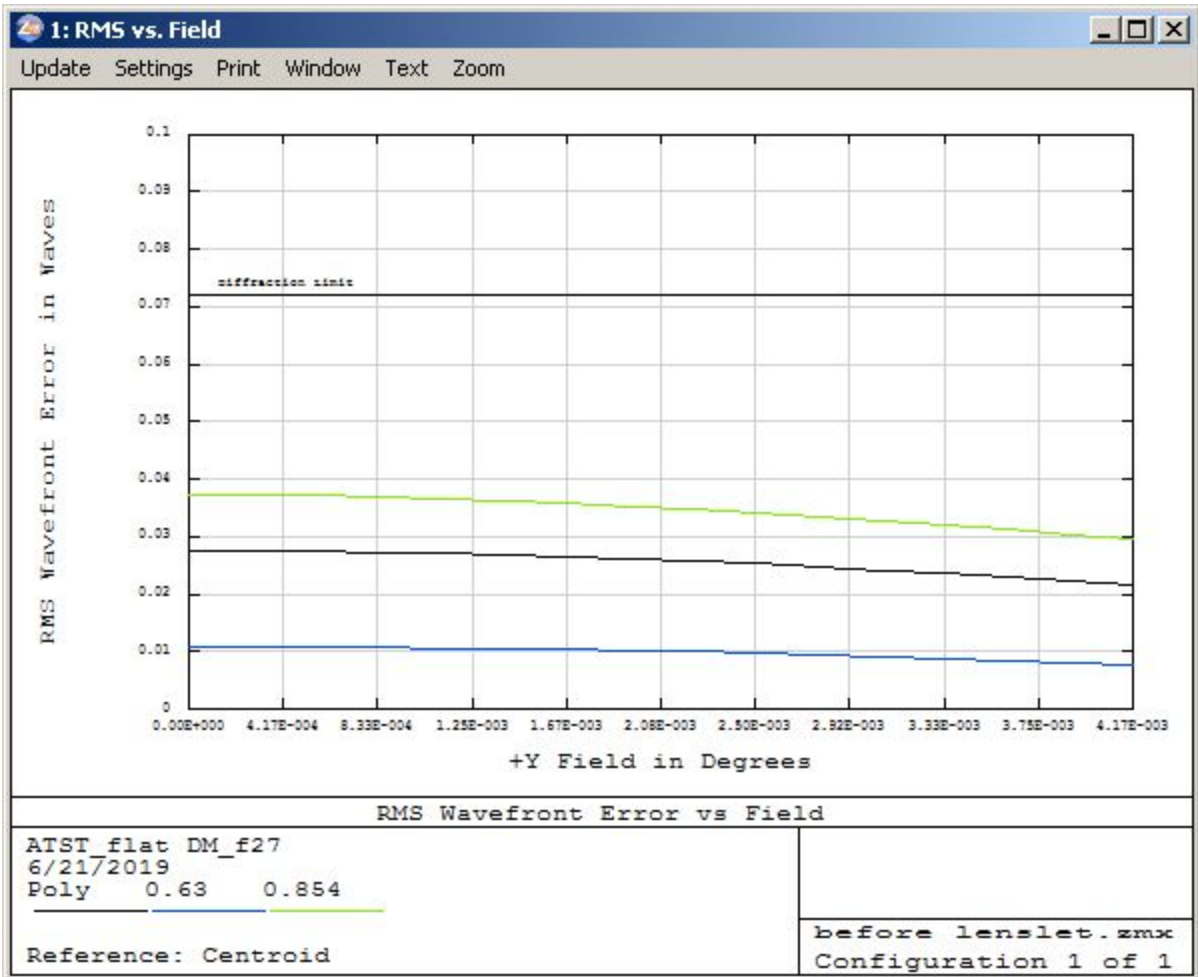


Fig 2.18 Best case RMS Wavefront Error for DKIST

Figure 2.18 displaying best RMS wavefront error attained with the RMS wavefront error 0.04 waves.

2.5.5 Design Parameters for Snapshot Spectrograph for DKIST

Table 2.12 Parameters and values for DKIST Spectrograph

Parameter	Worst Case Value	Best Case Value
Airy Disc Radius	12.54 μm	
Spot Size	18 μm	7 μm
Strehl Ratio	0.814	0.981
RMS Wavefront Error	0.08 waves	0.04 waves

2.5.6 Angle Distribution at image plane due to FP for DKIST

We have calculated angles at a 2k X 2k detector with 6.4 μm pixel size using the lenslet array as mentioned above.

Similar to the work we did for MAST, We have assumed the detector axis is aligned with the principal axis of the system and the Fabry Perot. We have calculated angles at each pixel from the line joining the center of the imaging lens and the pixel with the principal axis. To calculate the microlens array mask, as given in Table 2.4, we have used a 1.5 mm pitch microlens array, 300 mm focal length collimating lens and 300 mm focal length imaging lens. We infer that because the system is centrally symmetric, at same radial distances from the detector center, the angles will be the same, and Hence according to equation 2.2, all pixels at the same radial distance will be at the same wavelength. We also note that the maximum angular variation is 1.4 degrees. Figure 2.19 shows the angle variation on the detector with the microlens array masks.

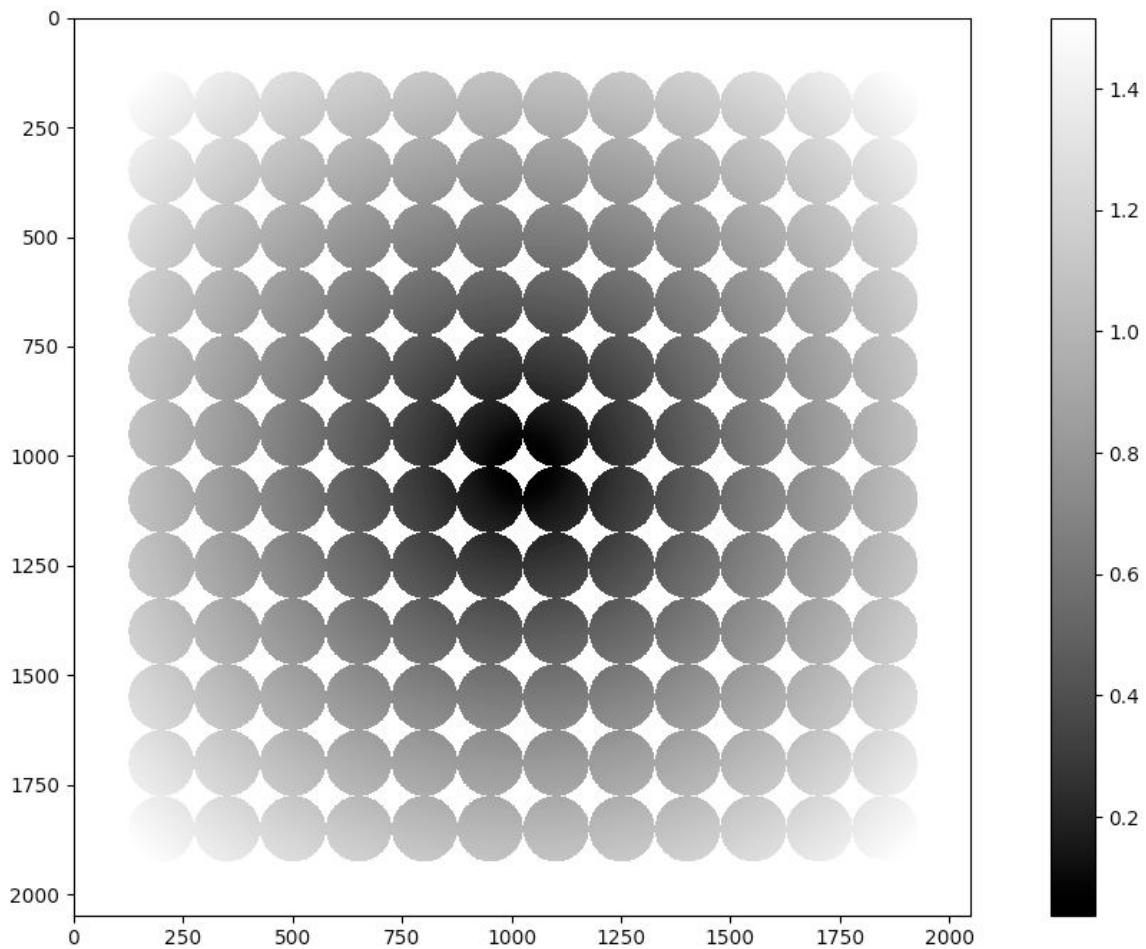


Fig 2.19 Angles in degrees on the Detector when 2k x 2k detector with 6.4 μm pixel size is used with microlens arrays with 1.5 mm pitch

2.6 Summary and Future Work

We have designed spectrograph designs for MAST and DKIST. For MAST we have used off-the-shelf components due to modest angular magnification and modest beam width provided to the back-end instruments by MAST. For DKIST, We have designed 2 custom achromats each to focus and to collimate the light. We are using off-the-shelf microlens array. We have also done the tolerance analysis over the radius of curvatures, tilt, and thickness and Abbe number. The future scope is to contact manufacturers with the calculated tolerances and further optimizations must be done as per manufacturing limitations. After the modifications instrument must be installed and calibrated.

3 Instrumentation

In the previous chapter, we have discussed the design aspects of pupil sampling Snapshot Spectrograph for MAST and DKIST. In this chapter, we discuss the realization of the snapshot spectrograph at MAST with the available components, the data reduction process and also about the snapshot spectro-polarimeter characterization at IIA Optics lab and its results.

3.1 Snapshot Spectrograph at MAST

We have used available components to set up the pupil sampling spectrograph at MAST and the following table lists the specifications. We have also characterized the Fabry Perot and the pre-filter.

Table 3.1 Optical Design specification of Snapshot Spectrograph installed at MAST

Element	Specification
Telescope (T) Aperture	90 mm
Telescope (T) Focal Length	849.9 mm
Field Stop	3 mm
L1 Focal Length	150 mm
SH Lenslet Pitch	1 mm
SH Lenslet Focal Length	45 mm
L2 Focal Length	180 mm
Fabry Perot Type	Air-Spaced Etalon
FP FSR and FWHM	3.75 Å and 235 mÅ
L3 Focal Length	300 mm
FOV	50 arcsec

3.2 Fabry Perot Etalon and Prefilter Calibration at MAST

To calculate the free spectral range and a full-width half maximum of FP and to find out the shift in the spectra, we had put the FP in front of the grating-based spectrograph and captured 11 frames with step size 100 from -500 to 500. Also, we have captured the pre-filter transmission profile which is plotted below.

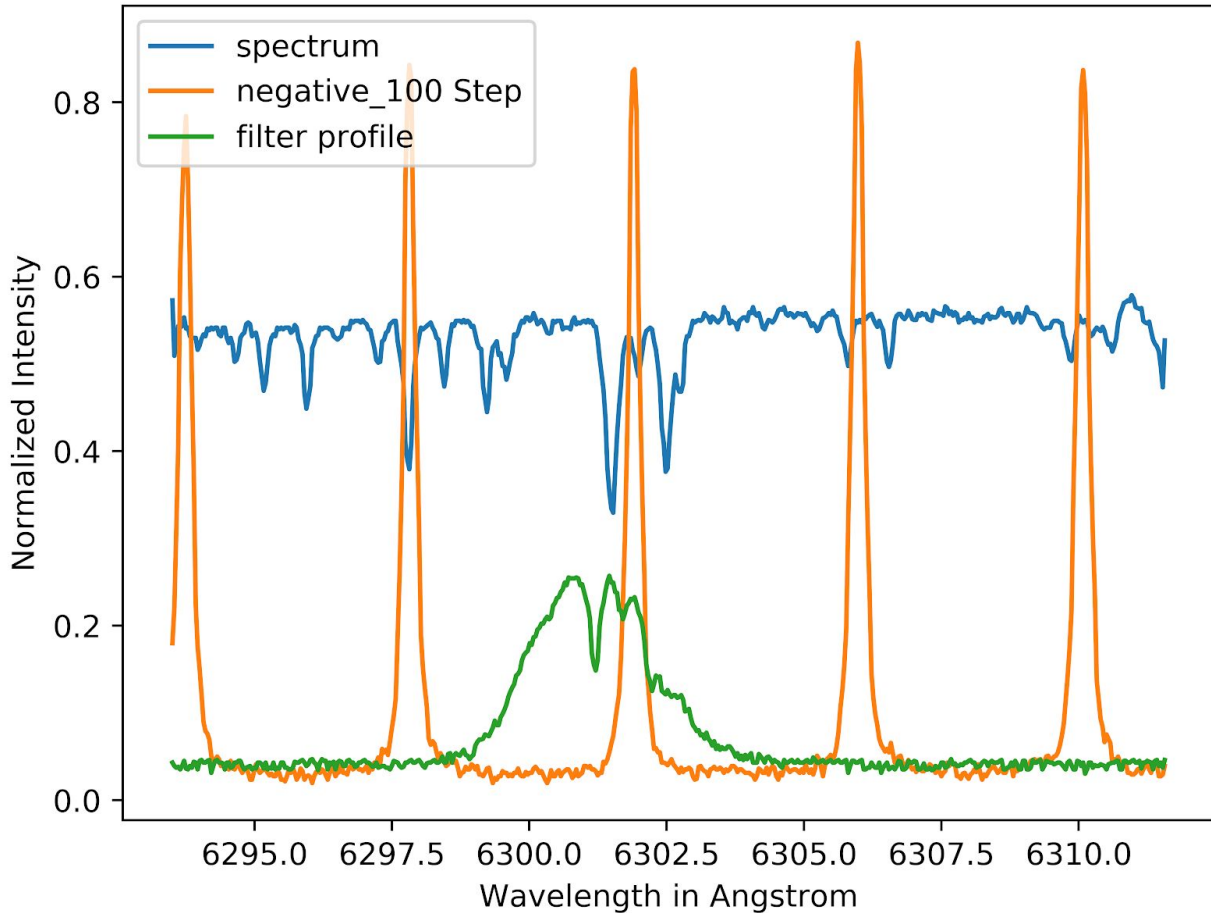


Fig 3.1 A sample FP profile at step -100 is overplotted with pre-filter profile and solar spectrum.

Table 3.2 FP Calibration Data

Quantity	Values
Free Spectral Range	3.75 Å
Full-Width Half Maximum	235 mÅ

Using the 11 data points about FP, we plotted the shift in spectra in wavelength we need to give to reference spectra (Step 0) for it to match the spectra at other steps. The graph shifts vs step number are plotted below.

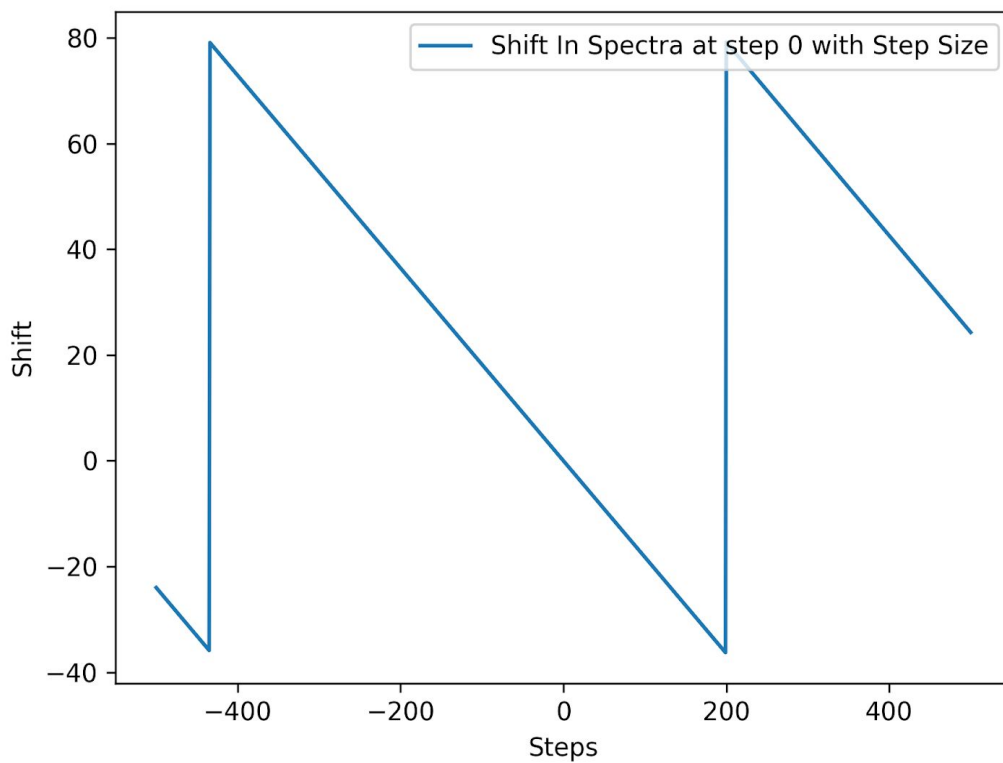


Fig 3.2 FP Shift in Spectra with respect to the spectrum at step 0 with step number

3.3 Instrument Setup

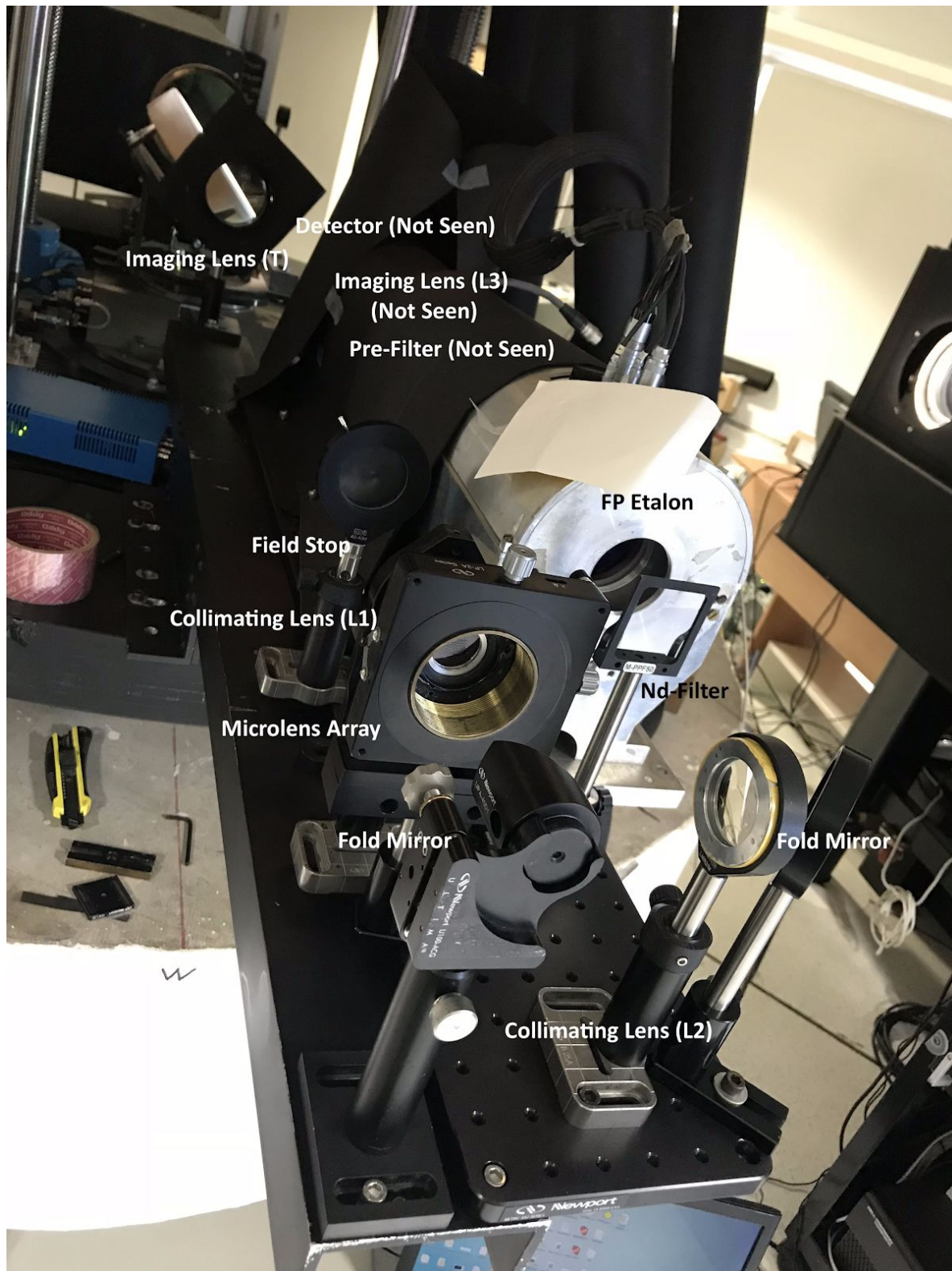


Fig 3.3 Photo Showing the experimental setup of Snapshot Spectrograph at MAST

Figure 3.3 shows the setup which consists of the imaging lens (T) followed by field stop. The beam is then collimated by the collimating lens (L1), which is making a pupil plane. The pupil plane is then sampled by microlens arrays. The fold mirror is folding the beam which is then collimated by collimating lens (L2). The beam is then again folded by fold mirror and passing through the Nd filter and then to the FP. the collimated beam from FP then passes through pre-filter followed by the imaging lens (L3) and gets imaged at the detector.

3.4 Data Reduction

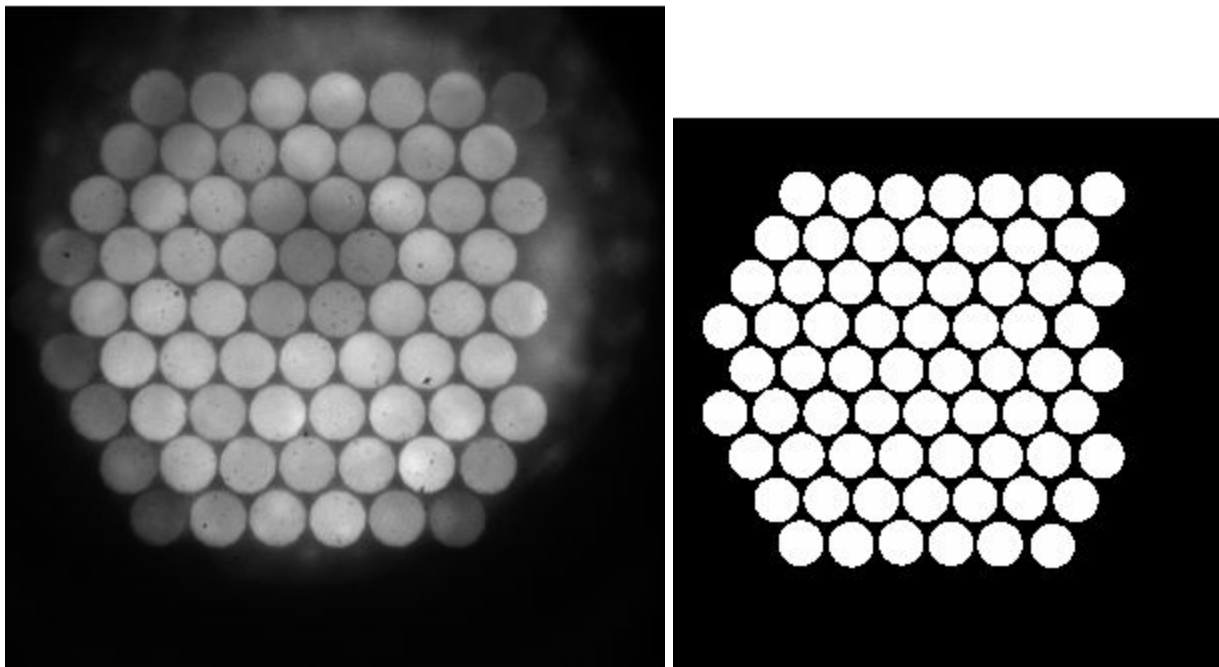


Fig 3.4 (a) spatio-spectral image plane (b) Mask for individual lenslet images by Hough Transform

A spatio-spectral image in x - y coordinates has a fixed wavelength for a given location (x_i, y_i) . Every (x_i, y_i) corresponds to a spatial region on the ROI of I_1 (Figure 3.4 (a)). A data cube of (x, y, λ) of the field can be built when spatially equivalent points (x_n, y_n) are identified and arranged in increasing or decreasing order of wavelength. In other words, a spatial region (x, y) is present at each image of the lenslet in the spatio-spectral image plane, and each is at a different wavelength. To identify each lenslet image in the detector, Hough transform is used and a mask is generated. (Figure 3.4 (b))

3.4.1 Flat Fielding

Flat fielding a snapshot spatio-spectral image plane requires tuning the FP to change the transmitted wavelength. As the spacing of FP changes, the center wavelength shifts, and the continuum will shift from pixel to pixel. Sampling all the pixels at continuum and averaging will generate the master flat for the spatio-spectral plane.

Due to alignment errors in the setup, the detector's center might not coincide with the principal axis and the center wavelength(λ_0) might be shifted from the spatio-spectral image plane center. To find the position of λ_0 , we trace the path of absorption lines in flat scan data by choosing a row along the x-axis and a column along the y-axis. Stacking the rows or columns for all the images gives an arc. Choosing points on the arc and fitting a circle will give us the position of the center wavelength in the spatio-spectral image plane (Figure 3.5 (a) and (b))

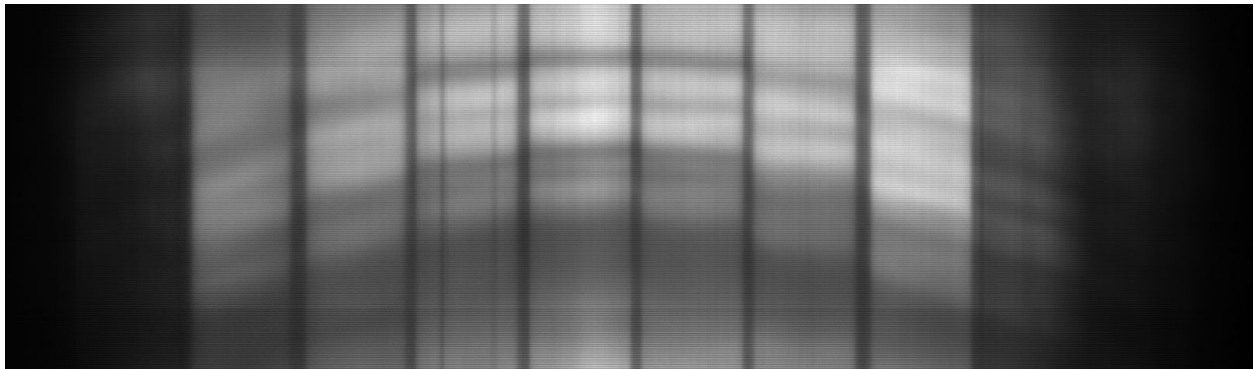


Fig 3.5 (a) Rows Stacked to trace the path of absorption lines

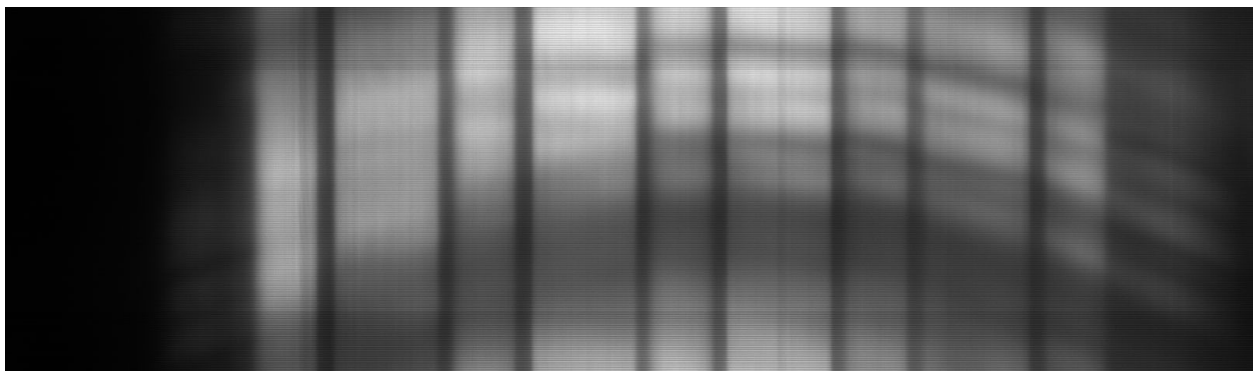


Fig 3.5 (b) Columns Stacked to trace the path of absorption lines

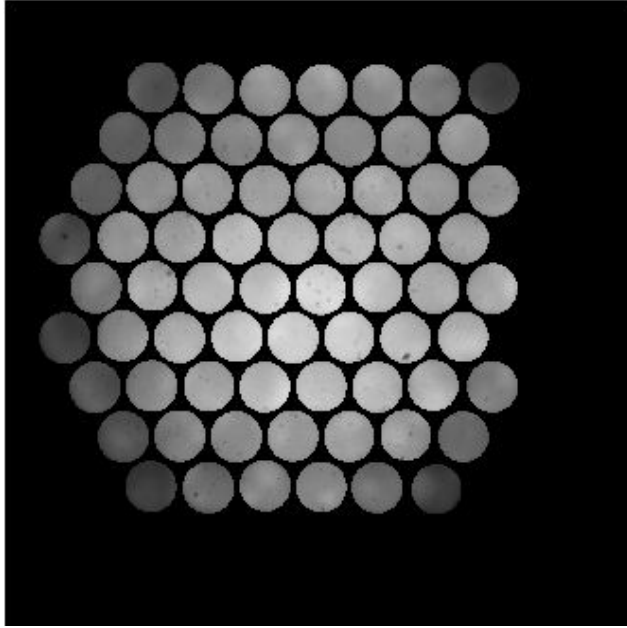


Fig 3.6 (a) Master Flat

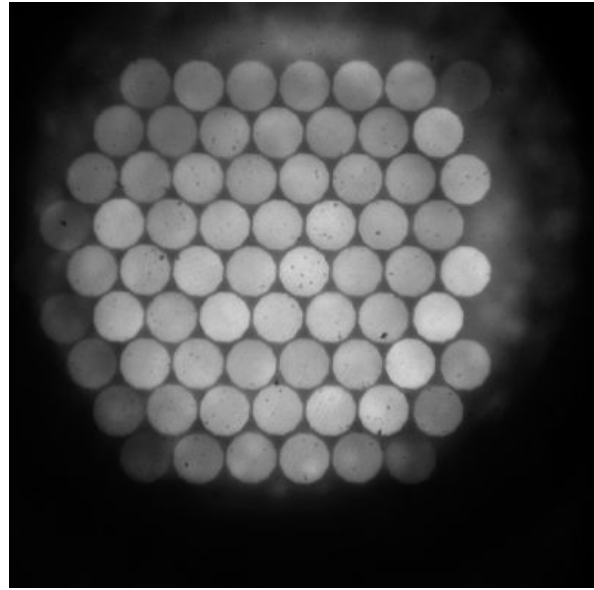


Fig 3.6 (b) Raw Data at step -150

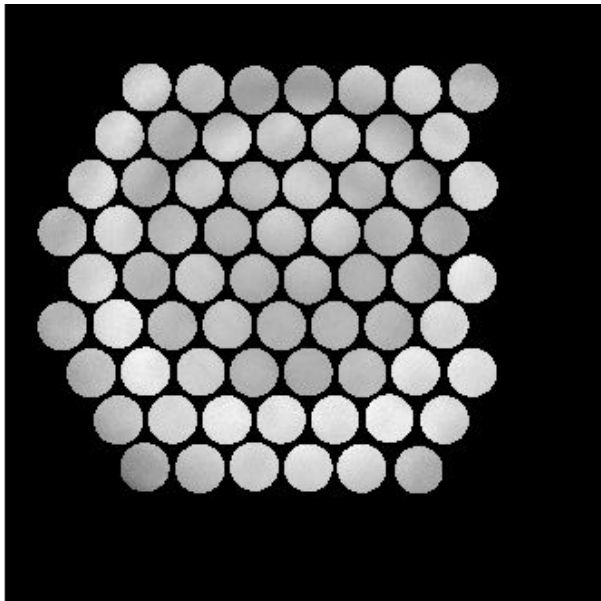


Fig 3.6 (c) Corrected Data at step -150

Figure 3.6 (a) shows the master flat generated from selecting pixels in the continuum wavelength region from the flat scans. Figure 3.6 (b) and (c) show a raw and a flat corrected image respectively.

3.4.2 Line Profile from Data

Due to bad observing conditions, we are unable to collect usable data. The data is with clouds passing by, which modulated the intensity and it is tough to separate cloud variations and variations due to FP.

We have plotted (Figure 3.7) the same graph of step -150 from the observed data. Although it does shows a reduced intensity at line 6301.5 Angstrom, it is not scientific data.

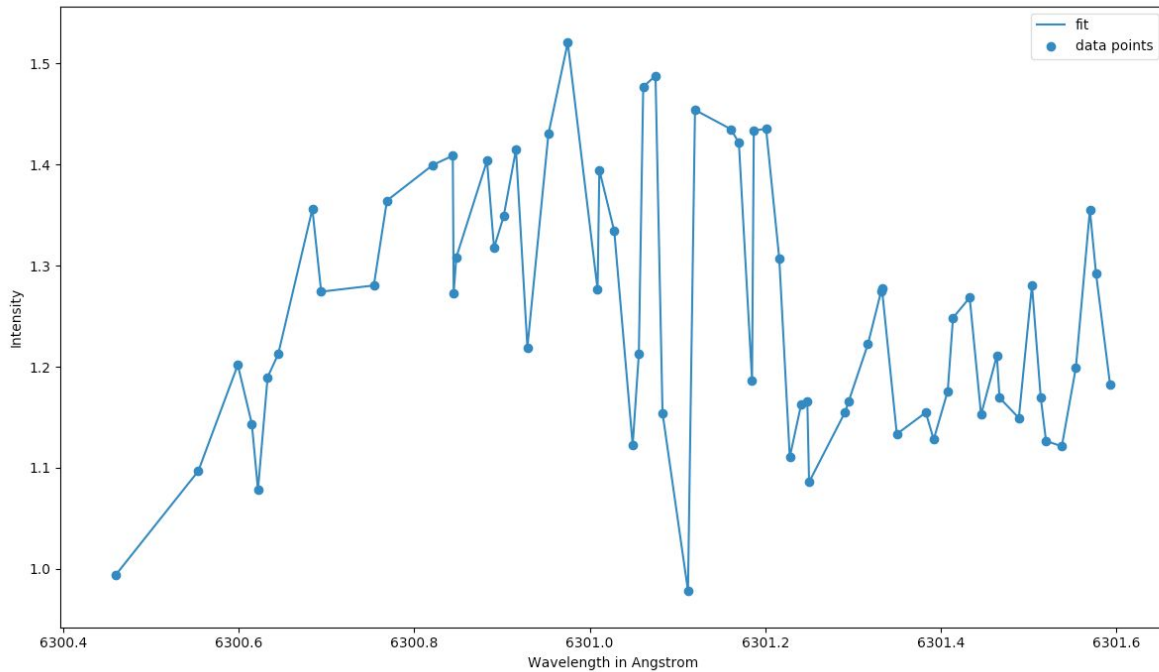


Fig 3.7 Line profile at a point using observed data at step -150

3.5 Simulated Data

We have calculated the wavelength incident at each pixel using the angle distribution at the detector (Figure 2.8) and equation 2.2. We have calculated the Intensity values for the wavelengths calculated using the BASS 2000 spectrum. Then we have multiplied the intensity values with the pre-filter profile and FP profile. At each step of the FP (spacing), the FP transmission is calculated using the shift vs step number plot (Figure 2.8). A sample simulated intensity profile is shown in Figure 3.8 for the FP step -150.

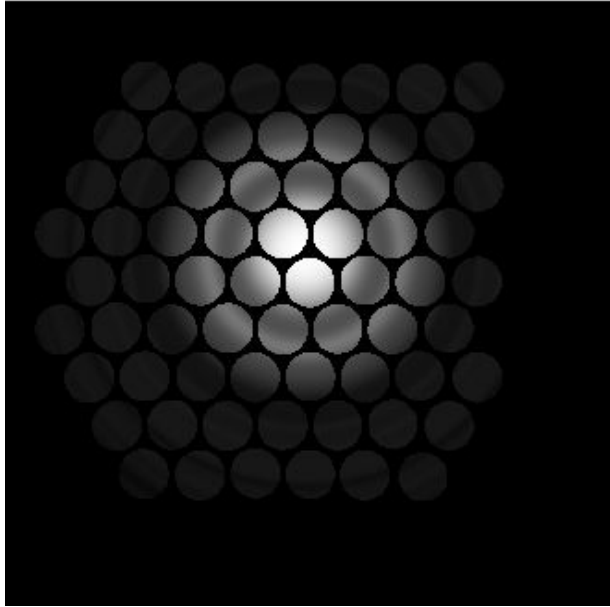


Fig 3.8 Simulated Data at step -150

3.5.1 Simulated Profile

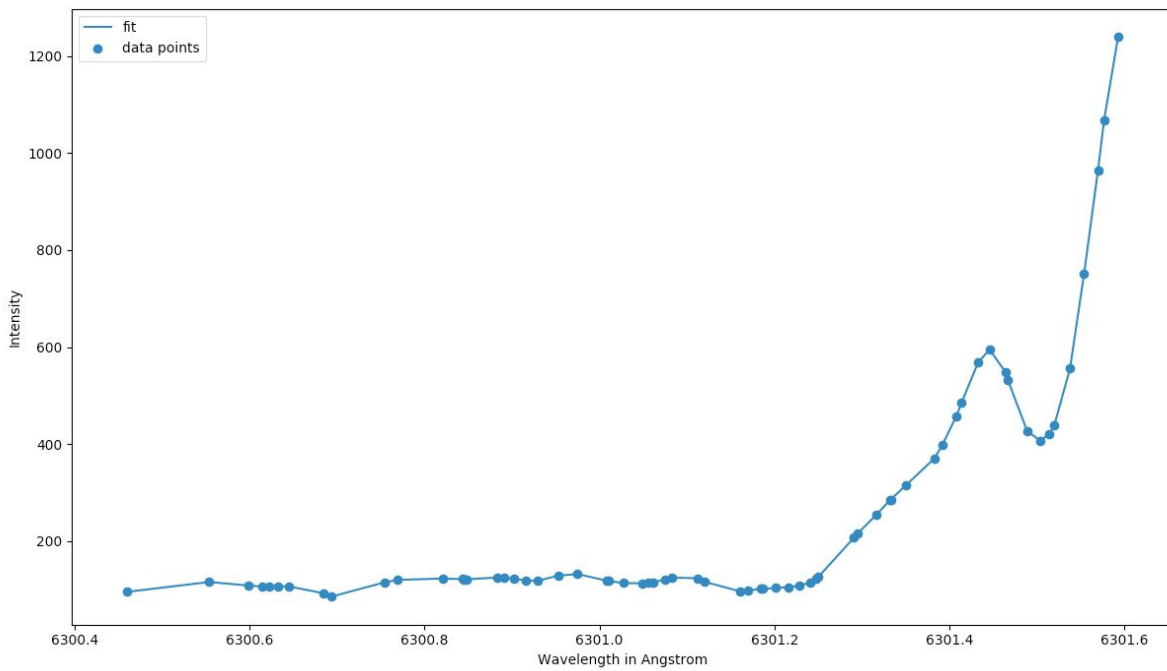


Fig 3.9 Line profile at a point using simulated data at step -150

Figure 3.9 displays a line profile at a spatial point using the simulated data. The filter response needs to be separated from this profile to get the appropriate line profile. We note that as expected line with center at 6301.538 is sampled with 8 wavelength points.

3.6 Snapshot Spectro-Polarimeter

We want to use this novel concept as a spectropolarimeter. Hence we had set up the snapshot spectro-polarimeter in IIA Optics lab and worked on the characterization of the polarimeter. We have used HeNe laser followed by a linear analyzer as a light source. The Linear analyzer is followed by a linear polarizer and a quarter wave plate being used together as Stokes polarimeter. It is then followed by a 50 μm pinhole. A 300 mm collimating lens then collimates the light and forms pupil plane at the focal plane. The microlens array is kept at the focal plane of the collimating lens which forms an image at 45 mm distance. The images from the microlens array are re-collimated by a 200 mm focal length lens, then the collimated beam is made to pass through the FP and reimaged by a 200 mm focal length lens at the detector. (Figure 3.10)

The following relations give the relation between intensity and the Stokes parameters.:

Intensity (x^0) signifies Intensity when the Linear polarizer of the polarimeter is kept x^0 from the horizontal.

$$\text{Stokes I} = \text{Intensity}(0^0) + \text{Intensity}(90^0)$$

$$\text{Stokes Q} = \text{Intensity}(0^0) - \text{Intensity}(90^0)$$

$$\text{Stokes U} = \text{Intensity}(45^0) - \text{Intensity}(135^0)$$

$$\text{Stokes V} = \text{Intensity}(\text{left circular}) - \text{Intensity}(\text{right circular})$$

3.6.1 Lab Snapshot Spectro-Polarimeter Setup

Table 3.3 Optical Design Specification of the Components used in IIA Optics Lab

Element	Specification
Laser Type	HeNe (632.8 nm)
Pinhole Size	50 μm
Collimating (L1) Lens Focal Length	300 mm
SH Lenslet Pitch	0.5 mm

SH Lenslet Focal Length	45 mm
L2 Focal Length	200 mm
Fabry Perot Type	Air-Spaced Etalon
FP FSR and FWHM	5.64 Å and 1.41 Å
L3 Focal Length	200 mm

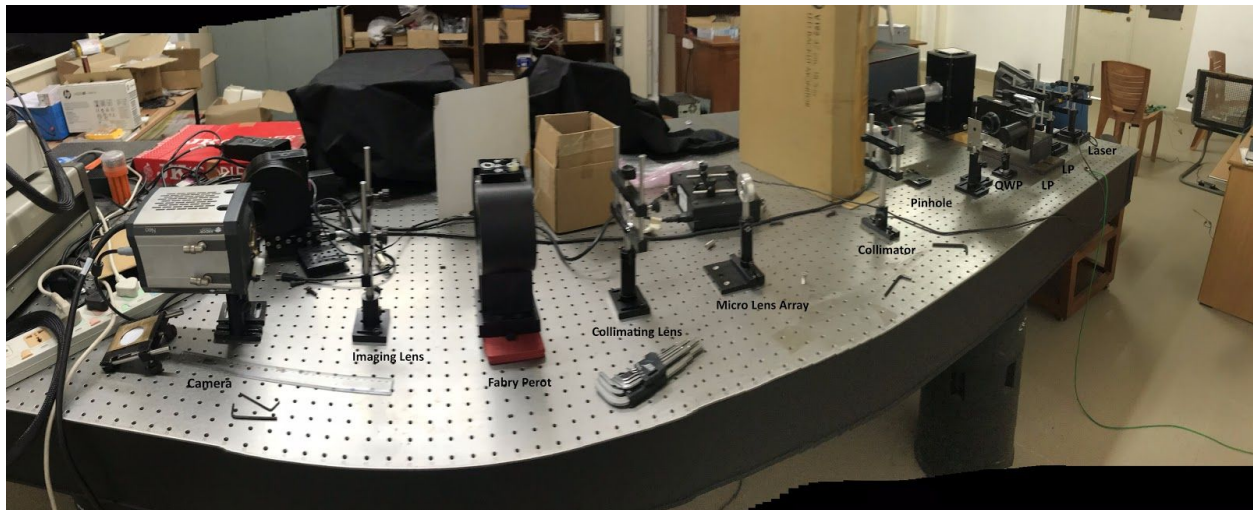


Fig 3.10 Snapshot Spectro-polarimeter Lab Setup

3.6.2 Data from Snapshot Polarimeter

We have collected data without FP and with FP to see the lenslet positions in the image plane.

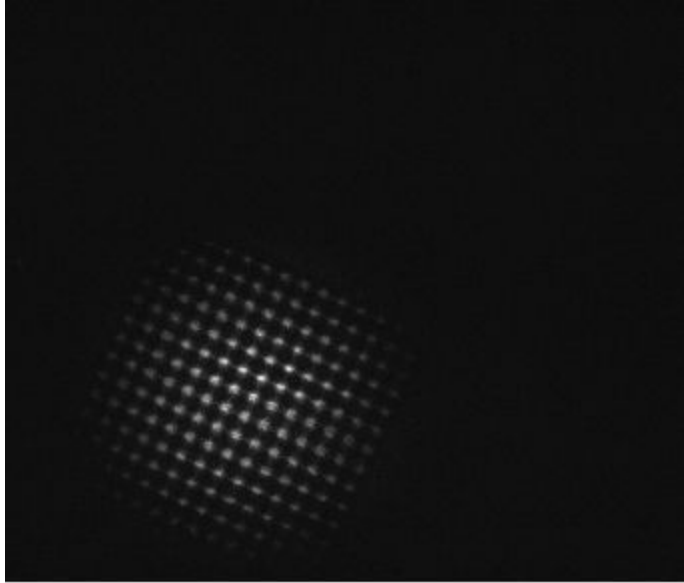


Fig 3.11 Lenslet images without FP



Fig 3.12 Data at Linear polarizer 0 degree orientation

Figure 3.11 shows the images of the lenslets when the FP is not present in the path. Hence we see all images from microlens array. Figure 3.12 shows the image from the snapshot spectrograph when the linear polarizer is at angle 0 degrees from the horizontal axis. We infer that the line is narrow and only the lenslets where HeNe wavelength(632.8 nm) wavelength fall upon are illuminated. In other words, The rest of the lenslet images are missing because they represent a wavelength not transmitted by the source. We also note that while taking these observations, we were unable to change X-parallelism of FP and hence unable to get it in operating mode. Hence the FP is used as is and FSR and FWHM can greatly differ than the values calculated earlier. For the same reason, we were unable to change the spacing too and

hence cannot estimate the center wavelength with the step number and cannot produce line profiles as produced in the MAST data. Only polarimeter data is presented here.

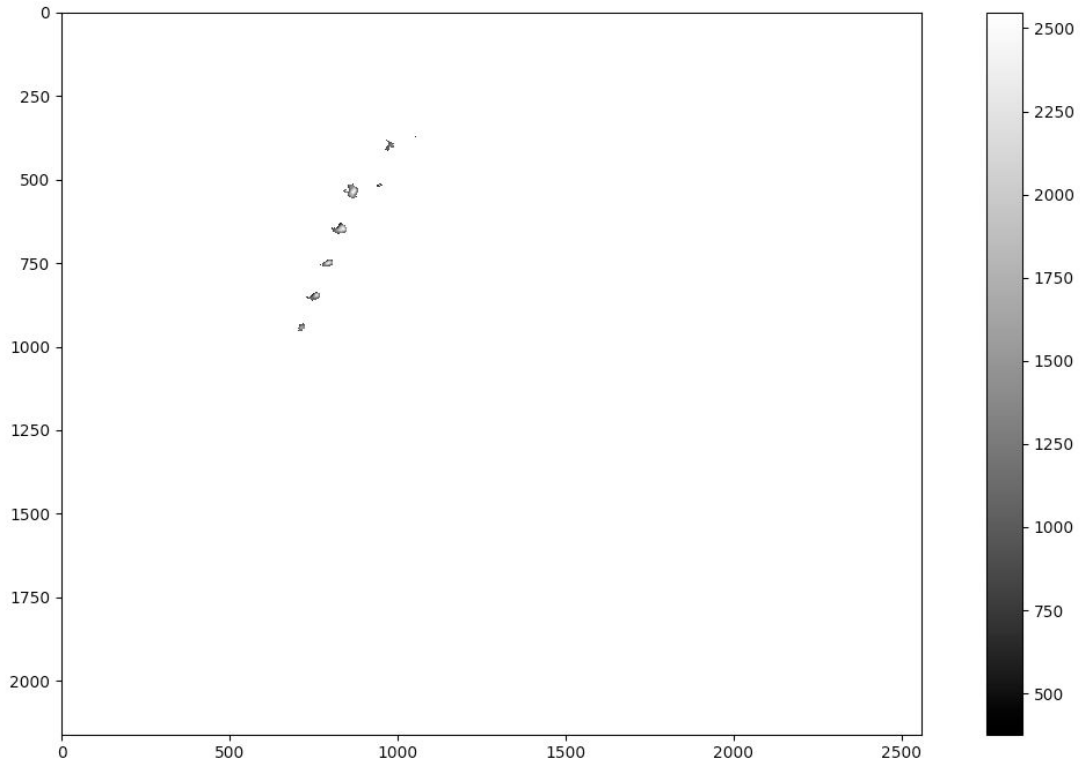


Fig 3.13 (a) Intensity Image at the detector for the linearly polarized He-Ne laser for the pixels at He-Ne passband.

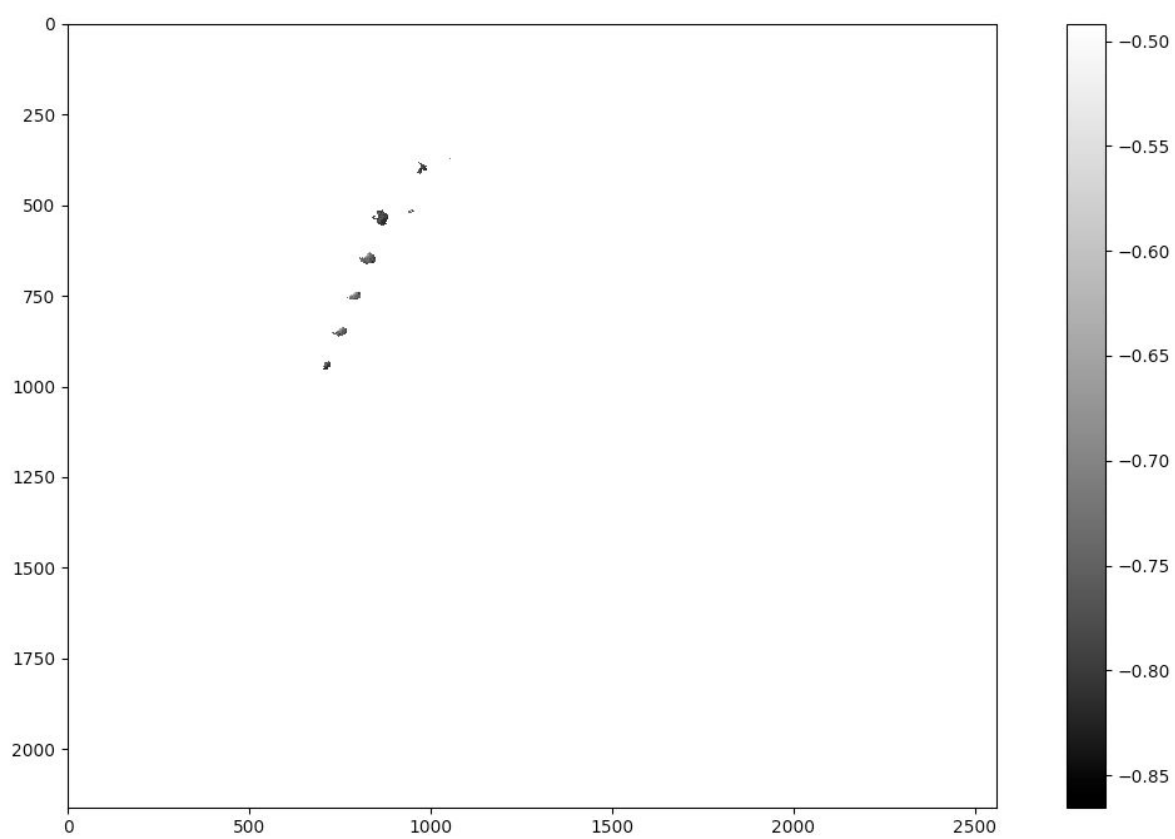


Fig 3.13 (b) Stokes Q/I for the linearly polarized He-Ne source at the detector for the pixels at He-Ne passband.

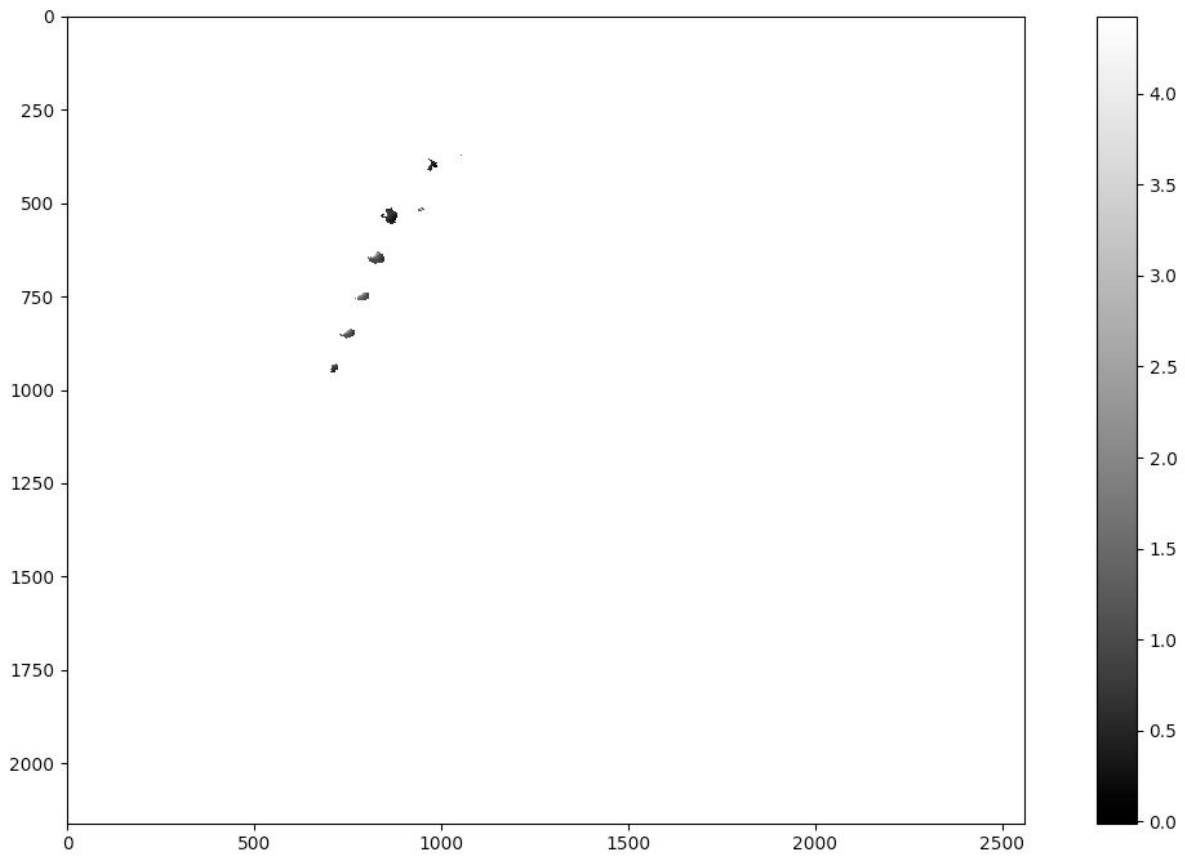


Fig 3.13 (c) Stokes U/I for the linearly polarized He-Ne source at the detector for the pixels at He-Ne passband.

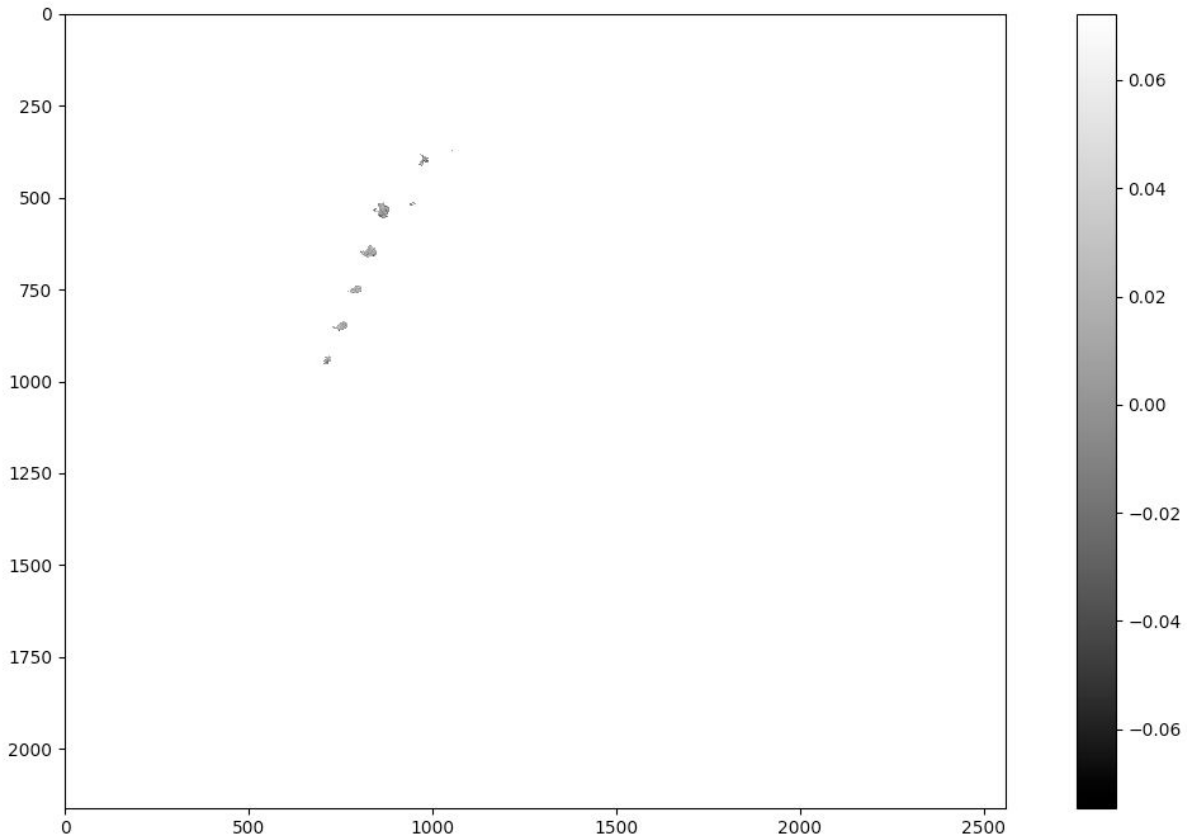


Fig 3.13 (d) Stokes V/I for the linearly polarized He-Ne source at the detector for the pixels at He-Ne passband.

The results (Figure 3.13 (a), (b), (c) and (d)) show Stokes Q as negative polarisation and Stokes U has a positive polarisation and Stokes V as zero. This indicates the light is coming at an angle given by $\tan^{-1}(\text{Stokes Q}/\text{Stokes U})$ to the horizontal axis and has no circular polarisation. The weak signal of Stokes V is present in the data due to inaccuracy in measurements which come while manually rotating the polarizer and waveplates.

3.7 Summary and Future Work

We have set up Snapshot Spectrograph at MAST Udaipur and Snapshot spectro-polarimeter at Optics Lab at IIA. The FP Calibration and observed profiles and simulated profiles are presented for the observed data. We have also simulated the BASS 2000 spectrum with prefilter and FP response and presented expected images and line profile. We have also set up the spectrograph and polarimeter at IIA Optics Lab and presented stokes parameter images. The initial results

show no circular polarization and show that light is linearly polarized at an angle to the horizontal.

The future work is to perform the same experiment using sunlight as a source and rotating stages or LCVR based polarimeter and characterize it for it to be used with telescopes like MAST or DKIST.

4 Summary and Future Work

The snapshot spectroscopy is performed by sampling the pupil plane using the microlens array to get multiple images of the field of view. The multiple images of FOV are then collimated and made to pass through an FP and a pre-filter. Further, the beam is imaged using an imaging lens to get multiple images of FOV on the detector with a blue shift in the spectrum as we move radially outwards the optic axis.

Using the above concept, we have made optimized designs of pupil sampling Snapshot Spectrograph for Multi Application Solar Telescope (MAST) and Daniel K. Inouye Solar Telescope (DKIST). For the MAST we have used all off-the-shelf components which can be readily purchased. For the DKIST, we have designed 4 lenses (2 collimators, 2 imagers). We have also provided the optimum distance between various surfaces, and also have done tolerance analysis and presented the results. The future scope is to contact the manufacturers and further optimize the design with the inputs of manufacturing limitations. Both designs should be realized and calibrated.

We have also demonstrated the working of the snapshot spectrograph using the available components at MAST. We have calibrated the FP using a grating based spectrograph and calculated the free spectral range, full-width half maximum and the shift in reference spectra with the step number. We have done a full scan over the FP spacing and collected some data. We have generated the master flat and also calculated the line center at the detector plane. We have also used the BASS 2000 spectrum to simulate the expected data from the instrument and plotted both the observed and expected profiles.

We have also set up the instrument in the IIA optics lab for the purpose of understanding the polarimetry. We have used laser followed by a linear analyzer as a light source and used a linear polarizer followed by a quarter-wave plate as Stokes definition polarimeter. We have presented the initial results i.e. Stokes parameters from this experiment and demonstrated that there is no circular polarization. The future work is to perform the same experiment using sunlight as a source and rotating stages or LCVR based polarimeter and characterize it for it to be used with telescopes like MAST or DKIST.

5 References

1. GMHJ Habets and J R W Heintze. “Empirical bolometric corrections for the main-sequence.” In: *Astronomy and Astrophysics Supplement Series* 46 (1981), pp. 193–237
2. Henny J. G. L. M. Lamers and Joseph P. Cassinelli. *Introduction to Stellar Winds*. May. Cambridge: Cambridge University Press, 1999, p. 24600. Doi: 10.1017/CBO9781139175012. URL: <http://ebooks.cambridge.org/ref/id/CBO9781139175012> (cit. on p. 1).
3. Hubbard, Robert, “DKIST Optical Prescription”, SPEC-0029 Rev G, 2015
4. Jan Jurcak, Manuel Collados, Jorrit Leenaarts, Michiel van Noort, Rolf Schlichenmaier. “Recent Advancements in EST” In: *Advances in Space Research*, Submitted Nov 2018.
5. S.K.Mathew. “A New 0.5m Telescope (MAST) for Solar Imaging and Polarimetry. In: *SOLAR POLARIZATION 5*, ASP Conference Series, Vol. 405, 2009
6. Jianwen Luo, Elisa E. Konofagou. “A Fast Normalized Cross-Correlation Calculation Method for Motion Estimation” In: *Ieee transactions on ultrasonics, ferroelectrics, and frequency control*, vol. 57, no. 6, June 2010,
7. Shibu K. Mathew, Ankala Raja Bayanna, Alok Ranjan Tiwary, Ramya Bireddy, Parameswaran Venkatakrishnan. “First Observations from the Multi-Application Solar Telescope (MAST) Narrow-Band Imager” In: *Solar Phys* (2017) 292:106, DOI 10.1007/s11207-017-1127-y
8. R. Mohanakrishna, K. Sankarasubramanian. “Lenslet Array and Fabry–Pérot-Based Hyperspectral Imaging Data Reduction Technique for Solar Observation” In: *Solar Phys* (2018) 293:108 <https://doi.org/10.1007/s11207-018-1331-4>
9. Alok Ranjan Tiwary, Shibu K. Mathew, A. Raja Bayanna, P. Venkatakrishnan, Rahul Yadav. “Imaging Spectropolarimeter for the Multi-Application Solar Telescope at Udaipur Solar Observatory: Characterization of Polarimeter and Preliminary Observations” In: *Solar Phys* (2017) 292:49 DOI 10.1007/s11207-017-1076-5
10. Mohanakrishna R. “HYPERSPETRAL AND SPECTROPOLARIMETRIC INSTRUMENTATION FOR THE SOLAR ATMOSPHERE” In: Thesis Submitted in 2017 Indian Institute of Science, Bangalore
11. J. Evershed. “Radial movement in sunspots.” In: *Monthly Notices of the Royal Astronomical Society* 69.5 (Mar. 1909), pp. 454– 458. doi: 10.1093/mnras/69.5.454.
12. Donald E. Jennings and R. J. Boyle. “Multichannel Fabry-Perot spectrometer for infrared astronomy.” In: *Applied Optics* 25.24 (Dec. 1986), p. 4520. doi: 10.1364/AO.25.004520.

13. C. Beck, W. Schmidt, T. Kentischer, D. Elmore. "Polarimetric Littrow Spectrograph – instrument calibration and first measurements". In: *A&A* 437, 1159–1167 (2005) DOI: 10.1051/0004-6361:20052662
14. Eric Hansen, Ron Price, Rob Hubbard. "Advanced Technology Solar Telescope optical design" In: *SPIE Astronomical Telescopes + Instrumentation*, 2006, Orlando, Florida , United States
15. K. Sankarasubramanian, Craig Gullixson, Stephen Hegwer, Thomas R. Rimmele, Scott Gregory, et al. "The Diffraction Limited Spectro- Polarimeter: a new instrument for high-resolution solar polarimetry". In: *Optical Science and Technology*, SPIE's 48th Annual Meeting, 2003, San Diego, California, United States
16. Michiel Van Noort, Luc Rouppe Van Der Voort, Mats G. Lofdahl. "Solar Image Restoration by use of multi-frame blind de-convolution with multiple objects and phase diversity". In: *Solar Physics* (2005) 228: 191–215
17. Mohanakrishna R, Sankarasubramaniam K, AND Bayanna A R "Lenslet array and Fabry-Perot based hyperspectral imaging" In: *The Astrophysical Journal*, 867:77 (7pp), 2018 November 1
18. K. Sankarasubramanian & Sanjay Gosain & P. Venkatakrishnan & A. Raja Bayanna. "A novel solar spectroscopic concept using Shack-Hartmann and Fabry-Perot" In: *J Opt* (April–June 2012) 41(2):114–116 DOI 10.1007/s12596-012-0074-0
19. D.P. Choudhary, S. Gosain, Comparative study of LiNbO₃ and servo controlled air gap Fabry-Perot etalons for solar application. *Exp. Astron.* 13, 153 (2002)

Appendix A

Analysis of Tolerances

File : E:\overall\before lenslet.zmx

Title: ATST_flat DM_f27

Date : 6/21/2019

Units are Millimeters.

All changes are computed using linear differences.

Paraxial Focus compensation only.

WARNING: Solves should be removed prior to tolerancing. Semi-diameters should be fixed.

WARNING: Boundary constraints on compensators will be ignored.

Criterion : RMS Spot Radius in Millimeters

Mode : Inverse Sensitivities, Limit Criterion Value : 0.01100000

Sampling : 2

Nominal Criterion : 0.00302148

Test Wavelength : 0.6328

Fields: XY Symmetric Angle in degrees

#	X-Field	Y-Field	Weight	VDX	VDY	VCX	VCY
1	0.000E+000	0.000E+000	4.000E+000	0.000	0.000	0.000	0.000
2	0.000E+000	4.125E-003	1.000E+000	0.000	0.000	0.000	0.000
3	0.000E+000	-4.125E-003	1.000E+000	0.000	0.000	0.000	0.000
4	0.000E+000	5.893E-003	1.000E+000	0.000	0.000	0.000	0.000
5	0.000E+000	-5.893E-003	1.000E+000	0.000	0.000	0.000	0.000
6	4.125E-003	0.000E+000	1.000E+000	0.000	0.000	0.000	0.000
7	-4.125E-003	0.000E+000	1.000E+000	0.000	0.000	0.000	0.000
8	5.893E-003	0.000E+000	1.000E+000	0.000	0.000	0.000	0.000
9	-5.893E-003	0.000E+000	1.000E+000	0.000	0.000	0.000	0.000

Sensitivity Analysis:

Type	Minimum			Maximum		
	Value	Criterion	Change	Value	Criterion	Change
TRAD 74 4.2722E-006	-0.12500000	0.00301723	-4.2534E-006	0.12500000	0.00302575	
TRAD 75 -1.7461E-005	-0.12500000	0.00303926	1.7785E-005	0.12500000	0.00300402	
TRAD 76 1.7828E-005	-0.12500000	0.00300402	-1.7454E-005	0.12500000	0.00303931	
TFRN 77 1.3255E-005	-0.12500000	0.00300843	-1.3049E-005	0.12500000	0.00303473	
TRAD 80 -6.4189E-006	-0.12500000	0.00302795	6.4722E-006	0.12500000	0.00301506	
TRAD 81 -1.3616E-005	-0.12500000	0.00303533	1.3856E-005	0.12500000	0.00300786	
TRAD 82 1.4257E-005	-0.12500000	0.00300747	-1.4006E-005	0.12500000	0.00303574	
TRAD 88 -1.0443E-005	-0.12500000	0.00303200	1.0519E-005	0.12500000	0.00301104	
TRAD 89 -4.9042E-005	-0.12500000	0.00308440	6.2926E-005	0.12500000	0.00297244	
TRAD 90 4.0752E-005	-0.12500000	0.00298190	-3.9575E-005	0.12500000	0.00306223	
TRAD 91 1.0645E-005	-0.12500000	0.00301456	-6.9152E-006	0.12500000	0.00303212	
TRAD 92 -7.6138E-006	-0.12500000	0.00303114	9.6585E-006	0.12500000	0.00301387	
TFRN 93 -1.0119E-006	-0.12500000	0.00302249	1.0159E-006	0.12500000	0.00302047	
TTHI 74 75 6.7939E-006	-0.05000000	0.00301475	-6.7287E-006	0.05000000	0.00302827	
TTHI 75 77 -6.5113E-006	-0.05000000	0.00302805	6.5757E-006	0.05000000	0.00301497	
TTHI 76 77 2.1786E-007	-0.05000000	0.00302126	-2.1782E-007	0.05000000	0.00302170	
TTHI 77 78 1.7781E-016	-0.05000000	0.00302148	3.3480E-016	0.05000000	0.00302148	

TTHI 78 79 -1.6610E-016	-0.05000000	0.00302148	-5.8547E-017	0.05000000	0.00302148
TTHI 79 82 -2.2998E-006	-0.05000000	0.00302379	2.3127E-006	0.05000000	0.00301918
TTHI 80 82 -2.0769E-006	-0.05000000	0.00302356	2.0857E-006	0.05000000	0.00301940
TTHI 81 82 -2.0935E-006	-0.05000000	0.00302359	2.1073E-006	0.05000000	0.00301939
TTHI 82 83 -1.2039E-012	-0.05000000	0.00302148	1.2031E-012	0.05000000	0.00302148
TTHI 83 84 1.6610E-006	-0.05000000	0.00301983	-1.6474E-006	0.05000000	0.00302314
TTHI 84 85 -7.5787E-006	-0.05000000	0.00302915	7.6727E-006	0.05000000	0.00301390
TTHI 85 86 -2.8189E-017	-0.05000000	0.00302148	9.5410E-018	0.05000000	0.00302148
TTHI 86 87 2.5934E-016	-0.05000000	0.00302148	9.4542E-017	0.05000000	0.00302148
TTHI 87 90 7.6706E-006	-0.05000000	0.00301390	-7.5775E-006	0.05000000	0.00302915
TTHI 88 90 7.9691E-008	-0.05000000	0.00302141	-6.6431E-008	0.05000000	0.00302156
TTHI 89 90 7.2241E-006	-0.05000000	0.00301430	-7.1756E-006	0.05000000	0.00302870
TTHI 90 93 1.6987E-009	-0.05000000	0.00302148	-1.6985E-009	0.05000000	0.00302148
TTHI 91 93 3.9776E-006	-0.05000000	0.00301764	-3.8405E-006	0.05000000	0.00302546
TTHI 92 93 -2.0994E-006	-0.05000000	0.00302358	2.1041E-006	0.05000000	0.00301938
TEDX 74 75 4.7611E-006	-0.05000000	0.00302620	4.7198E-006	0.05000000	0.00302624
TEDY 74 75 1.8288E-006	-0.05000000	0.00302434	2.8655E-006	0.05000000	0.00302331
TETX 74 75 -9.4959E-006	-0.05000000	0.00303170	1.0221E-005	0.05000000	0.00301198
TETY 74 75 7.6312E-007	-0.05000000	0.00302226	7.8140E-007	0.05000000	0.00302224

TEDX 76 77 3.5473E-006	-0.05000000	0.00302506	3.5798E-006	0.05000000	0.00302503
TEDY 76 77 2.2440E-006	-0.05000000	0.00302315	1.6734E-006	0.05000000	0.00302372
TETX 76 77 1.3485E-005	-0.05000000	0.00301374	-7.7425E-006	0.05000000	0.00303496
TETY 76 77 2.8497E-006	-0.05000000	0.00302428	2.8033E-006	0.05000000	0.00302433
TEDX 80 82 8.1155E-007	-0.01250000	0.00302167	1.9358E-007	0.02500000	0.00302229
TEDY 80 82 3.4696E-007	-0.05000000	0.00302135	-1.2720E-007	0.05000000	0.00302183
TETX 80 82 -3.9326E-008	-0.05000000	0.00302148	9.7709E-010	0.05000000	0.00302144
TETY 80 82 9.3871E-008	-0.05000000	0.00302156	8.4425E-008	0.05000000	0.00302157
TEDX 88 90 4.1774E-006	-0.05000000	0.00302562	4.1366E-006	0.05000000	0.00302566
TEDY 88 90 3.6648E-007	-0.05000000	0.00302940	7.9170E-006	0.05000000	0.00302185
TETX 88 90 2.0961E-005	-0.05000000	0.00306247	4.0995E-005	0.05000000	0.00304244
TETY 88 90 3.1031E-005	-0.05000000	0.00305262	3.1143E-005	0.05000000	0.00305251
TEDX 91 93 -1.0156E-008	-0.05000000	0.00302147	-1.0963E-008	0.05000000	0.00302147
TEDY 91 93 -2.7428E-009	-0.05000000	0.00302146	-1.9039E-008	0.05000000	0.00302148
TETX 91 93 2.0238E-005	-0.05000000	0.00306144	3.9960E-005	0.05000000	0.00304172
TETY 91 93 3.0154E-005	-0.05000000	0.00305173	3.0253E-005	0.05000000	0.00305163
TSDX 74 5.1760E-007	-0.05000000	0.00302198	5.0489E-007	0.05000000	0.00302200
TSDY 74 3.1406E-007	-0.05000000	0.00302167	1.9181E-007	0.05000000	0.00302179
TIRX 74 9.6826E-006	-0.00625000	0.00303111	9.6269E-006	0.00625000	0.00303116

TIRY 74	-0.02336744	0.00308974	6.8265E-005	0.02325541	0.00308771
6.6229E-005					
TSDX 75	-0.05000000	0.00302360	2.1201E-006	0.05000000	0.00302363
2.1486E-006					
TSDY 75	-0.05000000	0.00302311	1.6357E-006	0.05000000	0.00302196
4.7931E-007					
TIRX 75	-0.00625000	0.00303139	9.9080E-006	0.00625000	0.00303133
9.8467E-006					
TIRY 75	-0.02316361	0.00309449	7.3010E-005	0.02335861	0.00308588
6.4398E-005					
TSDX 76	-0.05000000	0.00302506	3.5798E-006	0.05000000	0.00302503
3.5473E-006					
TSDY 76	-0.05000000	0.00302315	1.6734E-006	0.05000000	0.00302372
2.2440E-006					
TIRX 76	-0.00625000	0.00303810	1.6625E-005	0.00625000	0.00303817
1.6696E-005					
TIRY 76	-0.02116722	0.00312363	0.00010215	0.02099356	0.00312666
0.00010519					
TSDX 77	-0.05000000	0.00302148	0.00000000	0.05000000	0.00302148
0.00000000					
TSDY 77	-0.05000000	0.00302148	0.00000000	0.05000000	0.00302148
-1.3010E-018					
TIRX 77	-0.00625000	0.00303778	1.6304E-005	0.00625000	0.00303772
1.6240E-005					
TIRY 77	-0.02123760	0.00312044	9.8960E-005	0.02133479	0.00312712
0.00010564					
TSDX 80	-0.02500000	0.00302159	1.1141E-007	0.02500000	0.00302160
1.2415E-007					
TSDY 80	-0.05000000	0.00302160	1.2141E-007	0.05000000	0.00302146
-2.0944E-008					
TIRX 80	-0.00312500	0.00302171	2.3375E-007	0.00312500	0.00302173
2.5201E-007					
TIRY 80	-0.05000000	0.00302745	5.9691E-006	0.05000000	0.00302906
7.5777E-006					
TSDX 81	-0.02500000	0.00302136	-1.1408E-007	0.02500000	0.00302136
-1.2371E-007					
TSDY 81	-0.05000000	0.00302171	2.3346E-007	0.05000000	0.00302335
1.8685E-006					

TIRX 81 -1.5201E-007	-0.00625000	0.00302132	-1.6312E-007	0.00625000	0.00302133
TIRY 81 2.6069E-005	-0.05000000	0.00304006	1.8580E-005	0.05000000	0.00304755
TSDX 82 1.5498E-008	-0.02500000	0.00302147	-5.2807E-009	0.02500000	0.00302149
TSDY 82 1.1075E-007	-0.05000000	0.00302261	1.1296E-006	0.05000000	0.00302159
TIRX 82 -4.7403E-009	-0.00156250	0.00302149	6.9753E-009	0.00156250	0.00302147
TIRY 82 4.5673E-005	-0.05000000	0.00307616	5.4684E-005	0.05000000	0.00306715
TSDX 88 3.4302E-006	-0.05000000	0.00302491	3.4294E-006	0.05000000	0.00302491
TSDY 88 5.5405E-006	-0.05000000	0.00302279	1.3122E-006	0.05000000	0.00302702
TIRX 88 0.00020184	-0.05000000	0.00322331	0.00020183	0.05000000	0.00322332
TIRY 88 0.00018620	-0.05000000	0.00323856	0.00021708	0.05000000	0.00320768
TSDX 89 5.3525E-005	-0.05000000	0.00307499	5.3513E-005	0.05000000	0.00307500
TSDY 89 4.4148E-005	-0.05000000	0.00308429	6.2812E-005	0.05000000	0.00306563
TIRX 89 0.00018675	-0.05000000	0.00320825	0.00018677	0.05000000	0.00320823
TIRY 89 0.00016975	-0.05000000	0.00322499	0.00020351	0.05000000	0.00319123
TSDX 90 2.6176E-005	-0.05000000	0.00304763	2.6149E-005	0.05000000	0.00304766
TSDY 90 2.9724E-005	-0.05000000	0.00304406	2.2583E-005	0.05000000	0.00305120
TIRX 90 0.00066652	-0.05000000	0.00368812	0.00066664	0.05000000	0.00368800
TIRY 90 0.00068221	-0.05000000	0.00367204	0.00065057	0.05000000	0.00370369
TSDX 91 2.5146E-005	-0.05000000	0.00304664	2.5163E-005	0.05000000	0.00304663

TSDY 91	-0.05000000	0.00303911	1.7635E-005	0.05000000	0.00305411
3.2632E-005					
TIRX 91	-0.05000000	0.00322975	0.00020827	0.05000000	0.00322971
0.00020823					
TIRY 91	-0.05000000	0.00325029	0.00022881	0.05000000	0.00320885
0.00018737					
TSDX 92	-0.05000000	0.00304766	2.6176E-005	0.05000000	0.00304767
2.6193E-005					
TSDY 92	-0.05000000	0.00305513	3.3649E-005	0.05000000	0.00304015
1.8675E-005					
TIRX 92	-0.04000000	0.00322743	0.00020595	0.04000000	0.00322738
0.00020590					
TIRY 92	-0.04000000	0.00324738	0.00022590	0.04000000	0.00320710
0.00018562					
TSDX 93	-0.05000000	0.00302148	0.00000000	0.05000000	0.00302148
0.00000000					
TSDY 93	-0.05000000	0.00302148	-4.3368E-019	0.05000000	0.00302148
0.00000000					
TIRX 93	-0.05000000	0.00380465	0.00078317	0.05000000	0.00380461
0.00078313					
TIRY 93	-0.05000000	0.00377827	0.00075679	0.05000000	0.00383062
0.00080914					
TIRR 74	-0.05000000	0.00306784	4.6358E-005	0.05000000	0.00297742
-4.4058E-005					
TIRR 75	-0.05000000	0.00297756	-4.3921E-005	0.05000000	0.00306768
4.6206E-005					
TIRR 76	-0.05000000	0.00307143	4.9955E-005	0.05000000	0.00297420
-4.7276E-005					
TIRR 77	-0.05000000	0.00297439	-4.7084E-005	0.05000000	0.00307122
4.9741E-005					
TIRR 80	-0.05000000	0.00302343	1.9544E-006	0.05000000	0.00301953
-1.9479E-006					
TIRR 81	-0.05000000	0.00302229	8.1070E-007	0.05000000	0.00302067
-8.0970E-007					
TIRR 82	-0.05000000	0.00301852	-2.9563E-006	0.05000000	0.00302445
2.9705E-006					
TIRR 88	-0.05000000	0.00304870	2.7225E-005	0.05000000	0.00299525
-2.6227E-005					

TIRR 89	-0.05000000	0.00302617	4.6890E-006	0.05000000	0.00301682
-4.6579E-006					
TIRR 90	-0.05000000	0.00299080	-3.0679E-005	0.05000000	0.00305353
3.2055E-005					
TIRR 91	-0.05000000	0.00304978	2.8304E-005	0.05000000	0.00299424
-2.7235E-005					
TIRR 92	-0.05000000	0.00302968	8.2011E-006	0.05000000	0.00301337
-8.1054E-006					
TIRR 93	-0.05000000	0.00298633	-3.5149E-005	0.05000000	0.00305846
3.6979E-005					
TIND 74	-0.00025000	0.00309808	7.6599E-005	0.00025000	0.00295070
-7.0779E-005					
TIND 76	-0.00025000	0.00297704	-4.4435E-005	0.00025000	0.00306839
4.6915E-005					
TIND 80	-0.00025000	0.00300677	-1.4707E-005	0.00025000	0.00303642
1.4939E-005					
TIND 81	-0.00025000	0.00302647	4.9931E-006	0.00025000	0.00301651
-4.9650E-006					
TIND 88	-0.00025000	0.00296817	-5.3308E-005	0.00025000	0.00307684
5.5357E-005					
TIND 89	-0.00025000	0.00304878	2.7299E-005	0.00025000	0.00299550
-2.5984E-005					
TIND 91	-0.00025000	0.00302957	8.0898E-006	0.00025000	0.00301554
-5.9364E-006					
TIND 92	-0.00025000	0.00301947	-2.0051E-006	0.00025000	0.00302483
3.3537E-006					
TABB 74	-0.17099667	0.00307828	5.6804E-005	0.17099667	0.00296527
-5.6212E-005					
TABB 76	-0.11989556	0.00296095	-6.0532E-005	0.11989556	0.00308206
6.0585E-005					
TABB 80	-0.16554989	0.00302020	-1.2828E-006	0.16554989	0.00302280
1.3214E-006					
TABB 81	-0.07133162	0.00302295	1.4668E-006	0.07133162	0.00302007
-1.4044E-006					
TABB 88	-0.14497603	0.00321078	0.00018930	0.14497603	0.00286506
-0.00015642					
TABB 89	-0.08062801	0.00285329	-0.00016819	0.08062801	0.00322625
0.00020477					

TABB 91	-0.16041834	0.00318292	0.00016144	0.16041834	0.00287874
	-0.00014274				
TABB 92	-0.08062801	0.00286109	-0.00016038	0.08062801	0.00320395
	0.00018247				

Worst offenders:

Type	Value	Criterion	Change
TIRY 93	0.05000000	0.00383062	0.00080914
TIRX 93	-0.05000000	0.00380465	0.00078317
TIRX 93	0.05000000	0.00380461	0.00078313
TIRY 93	-0.05000000	0.00377827	0.00075679
TIRY 90	0.05000000	0.00370369	0.00068221
TIRX 90	-0.05000000	0.00368812	0.00066664
TIRX 90	0.05000000	0.00368800	0.00066652
TIRY 90	-0.05000000	0.00367204	0.00065057
TIRY 91	-0.05000000	0.00325029	0.00022881
TIRY 92	-0.04000000	0.00324738	0.00022590

Estimated Performance Changes based upon Root-Sum-Square method:

Nominal RMS Spot Radius : 0.00302148
 Estimated change : 0.00162596
 Estimated RMS Spot Radius : 0.00464744

Compensator Statistics:

Change in back focus:

Minimum : -0.421662
 Maximum : 0.421961
 Mean : 0.000007
 Standard Deviation : 0.063596

Monte Carlo Analysis:

Number of trials: 20

Initial Statistics: Normal Distribution

Trial	Criterion	Change
1	0.00408991	0.00106844

2	0.00408170	0.00106022
3	0.00386850	0.00084703
4	0.00344188	0.00042040
5	0.00463250	0.00161102
6	0.00380584	0.00078436
7	0.00370181	0.00068033
8	0.00436118	0.00133970
9	0.00372546	0.00070398
10	0.00380239	0.00078091
11	0.00413767	0.00111619
12	0.00494680	0.00192532
13	0.00335044	0.00032896
14	0.00423423	0.00121275
15	0.00351115	0.00048967
16	0.00511829	0.00209681
17	0.00394608	0.00092460
18	0.00351736	0.00049588
19	0.00395451	0.00093303
20	0.00413215	0.00111067

Number of traceable Monte Carlo files generated: 20

Nominal 0.00302148
Best 0.00335044 Trial 13
Worst 0.00511829 Trial 16
Mean 0.00401799
Std Dev 0.00046074

Compensator Statistics:

Change in back focus:

Minimum : -0.552143

Maximum : 0.726911

Mean : 0.010367

Standard Deviation : 0.317345

90% > 0.00478965

80% > 0.00429770

50% > 0.00395029

20% > 0.00360959

10% > 0.00347651

End of Run.